AD NUMBER

AD474410

LIMITATION CHANGES

TO:

Approved for public release; distribution is unlimited.

FROM:

Distribution authorized to U.S. Gov't. agencies and their contractors; Administrative/Operational Use; NOV 1965. Other requests shall be referred to Air Force Arnold Engineering Development Center, AEDC-IN (STINFO), 251 First Street, Arnold AFB, TN 38389-2305.

AUTHORITY

aedc per dtic form 55

AEDC-TR-65-228

Nelius

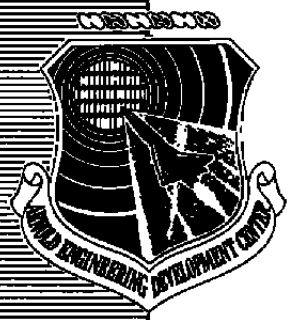

MEASUREMENT OF NONAXIAL FORCES PRODUCED BY SOLID-PROPELLANT ROCKET MOTORS USING A SPIN TECHNIQUE

M. A. Nelius and J. E. Harris

ARO, Inc.

November 1965

ROCKET TEST FACILITY

ARNOLD ENGINEERING DEVELOPMENT CENTER

AIR FORCE SYSTEMS COMMAND

ARNOLD AIR FORCE STATION, TENNESSEE

NOTICES

When U. S. Government drawings specifications, or other data are used for any purpose other than a definitely related Government procurement operation, the Government thereby incurs no responsibility nor any obligation whatsoever, and the fact that the Government may have formulated, furnished, or in any way supplied the said drawings, specifications, or other data, is not to be regarded by implication or otherwise, or in any manner licensing the holder or any other person or corporation, or conveying any rights or permission to manufacture, use, or sell any patented invention that may in any way be related thereto.

Qualified users may obtain copies of this report from the Defense Documentation Center.

References to named commercial products in this report are not to be considered in any sense as an endorsement of the product by the United States Air Force or the Government.

Defense Documentation Center release to the Clearinghouse for Federal Scientific and Technical Information (CFSTI) and foreign announcement and distribution of this report are not authorized. The distribution of this report is limited because it contains technology identifiable with items excluded from export by the Department of State.

MEASUREMENT OF NONAXIAL FORCES PRODUCED BY SOLID-PROPELLANT ROCKET MOTORS USING A SPIN TECHNIQUE

M. A. Nelius and J. E. Harris
ARO, Inc.

FOREWORD

The work reported herein was sponsored by Arnold Engineering Development Center (AEDC), Air Force Systems Command (AFSC), Arnold Air Force Station, Tennessee, under Program Element 65402234.

The results of research presented were obtained by ARO, Inc. (a subsidiary of Sverdrup and Parcel, Inc.), contract operator of AEDC under Contract AF 40(600)-1200. The research was conducted in Propulsion Engine Test Cell (T-3) of the Rocket Test Facility (RTF) under ARO Project No. RT8002, and the manuscript was submitted for publication on October 12, 1965.

The authors wish to acknowledge the efforts of Paul M. Hood, Manager, T-Projects Branch, Rocket Test Facility. Mr. Hood conceived the idea of measuring nonaxial forces using the spin technique.

This technical report has been reviewed and is approved.

Ralph W. Everett
Major, USAF
AF Representative, RTF
DCS/Test

Jean A. Jack
Colonel, USAF
DCS/Test

ABSTRACT

This report introduces a technique for measurement of nonaxial forces produced by solid-propellant rocket motors which is independent of thrust stand interactions and motor weight variations. The technique consists of measuring the axial and two horizontal transverse forces (three components) while spinning the motor about its axial centerline. The accuracy of radial force measurement using the spin technique was established from a dynamic transverse force calibration which was accomplished in the presence of a 4800-lb_f, thrust-simulating axial load. It was determined that radial forces having magnitudes less than 10 lb_f could be determined within 0.5 lb_f and that radial forces greater than 10 lb_f could be determined within 5 percent at rotational speeds up to 250 rpm. The principle of the technique, its limitations, and advantages are discussed. Details of the dynamic transverse force calibrations and test results of nonaxial force measurements during motor firings are also presented.

CONTENTS

ILLUSTRATIONS

Figure

NOMENCLATURE

F	Force, lb_f
F_{cent}	Calculated centrifugal force, $F_{cent} = mr\omega^2$, lb_f
F_{pred}	Calibration force magnitude, $F_{pred} = (MF)\, F_{cent}$, lb_f
MF	Forced vibration magnification factor
m	Unbalance mass, lb_m
r	Unbalance eccentricity, in.

t	Time, sec
ζ	Damping factor
θ	Angular coordinate of rotating system, deg
ϕ	Angular phase lag, deg
ω	Rotational speed

SUBSCRIPTS

d, u	Condition at downstream and upstream axial measuring stations
f	Electronic filter effect
n	Condition at resonance
t	Vector summation of forces at stations u and d
v	Forced vibration effect

SECTION I
INTRODUCTION

The extent to which the thrust vector of a solid-propellant rocket motor is misaligned from the motor axial centerline is of great significance for many space applications where precision trajectory requirements exist. Nonaxial force measurement has, heretofore, been accomplished through testing on a multicomponent thrust stand which requires that the six components (Fig. 1), which define the force system, be individually measured. This method, however, has several inherent complexities which necessitate large corrections to the measured force data. Primary among these corrections are those necessary to account for motor weight variations with time and for thrust stand interactions which produce biased force measurements. A precise knowledge of the variation in motor weight and center-of-gravity location with time as well as the characteristics of the thrust stand is essential for accurate force measurement.

A technique for nonaxial force measurement which circumvents the aforementioned complexities was devised by personnel of the Rocket Test Facility, Arnold Engineering Development Center. The method consists of measuring the axial thrust and two horizontal transverse forces (three components) while rotating the motor about its horizontally oriented axial centerline. The spin method eliminates the two vertical force measuring systems required in the six-component stand method since, during one revolution of the test motor, the radial component of the thrust vector is twice located precisely in the horizontal plane. In addition, thrust stand interactions are inconsequential since the magnitude of the nonaxial force is proportional only to the double amplitude (forced difference) of the sinusoidally varying load cell output signal. However, the spin method of side force measurement assumes that the misaligned thrust vector intersects the spin axis and thus does not account for the roll component of the force system.

A dynamic transverse force calibration was performed in Propulsion Engine Test Cell (T-3) of the Rocket Test Facility to determine the accuracy of force measurements using the spin technique. The calibration force was generated by an eccentrically mounted mass which, when rotated about the spin axis, produced a radially directed centrifugal force of known (calculated) magnitude. Data were obtained at various rotational speeds with three levels of imparted unbalance.

This report presents a discussion of the apparatus and operational principles used with the spin technique for nonaxial force measurement.

The configuration and results of the dynamic force calibration conducted as part of the system checkout are discussed. Transverse force measurements obtained during solid-propellant motor firings, accomplished at rotational speeds of 100 and 200 rpm, are presented.

SECTION II
APPARATUS AND OPERATIONAL PRINCIPLES

The test configuration for spin technique transverse force measurements consists of a horizontally oriented thrust cradle supported vertically by three double-flexure columns (Fig. 2). The cradle is restrained in the horizontal plane by one axial and two transverse columns, each containing a flexure-mounted, force-measuring load cell. The test motor is supported by forward and aft bearing assemblies and is rotated by an electric drive motor mounted on the cradle. The basic spin rig in Propulsion Engine Test Cell (T-3) (Ref. 1) was designed to accommodate motors having diameters up to 36 in. with maximum lengths up to approximately 120 in.

Nonaxial force measurement is accomplished by measuring forces in a horizontal plane and perpendicular to the motor centerline at two axial locations while rotating the motor about its axial centerline (Fig. 3). The angular location (θ) defining the direction of the nonaxial force component (F_t) can be determined through motor rotation since the traversing, radially directed motor force vector will produce a sinusoidal output from the two transverse force measuring systems. The transverse component of the motor thrust vector (F_t) is located in the horizontal plane at the times when F_u and F_d (Fig. 3) are either maximum or minimum. The magnitude and axial position of F_t can be determined by properly summing the system forces and moments at times when F_t is in the horizontal plane. Examples of the expected variation in F_u and F_d with time for two axial locations of F_t and the corresponding methods of calculation are shown in Fig. 4.

The spin technique for nonaxial force measurement has two significant advantages over the six-component stand method. The motor weight change correction, which must be applied to the measured vertical forces when using the six-component method and which can be as much as two orders of magnitude greater than the force which is to be measured, is not required with the spin technique since all forces are measured in the horizontal plane. Thrust stand interactions do not affect the transverse force measurements since the spin technique depends only on a force difference (not absolute value). For example, with no interaction and a constant motor

nonaxial force, the outputs from the transverse force measuring system will oscillate sinusoidally about zero with the values of maximum and minimum forces being equal in magnitude but opposite in sign (Fig. 5a). However, when interaction effects are present, the sine wave is displaced by an amount which is dependent upon the degree of interaction present (Fig. 5b). The magnitude of the nonaxial force is equal to one-half of the algebraic difference between the maximum and succeeding minimum measured force. The magnitude of the thrust stand interaction effect is one-half of the algebraic sum of a maximum and succeeding minimum measured force. It can be seen from the above discussion that the nonaxial force component is derived from a signal at least twice as great as that which would be measured by a six-component method. For example, with the six-component stand the signal generated by the transverse force is distributed between four load cells (neglecting roll). With the spin technique, a double amplitude signal is distributed between only two measuring stations, thereby contributing toward improved system data accuracy.

Assumptions and corrections associated with the spin method for measuring transverse forces are: The data must be corrected for system centrifugal unbalance forces resulting from spinning. The technique assumes that any variation in the direction and magnitude of the transverse vector will be small during each revolution of the test motor. It is assumed that nonaxial forces intersect the spin axis, and thus the roll component of the force system is neglected. The unbalance correction can be minimized by testing at low spin rates (since centrifugal force is proportional to the square of rotational speed) and by precise balancing of the unit prior to test.

SECTION III
CALIBRATION

The accuracy of force measurement which might be expected using the spin technique was determined from a dynamic force calibration. The calibration consisted of rotating an eccentrically mounted weight about the spin axis, thereby producing a calculable centrifugal force. Data were obtained at various rotational speeds with three levels of imparted unbalance. This section presents a discussion of the calibration configuration, instrumentation, and results.

3.1 CONFIGURATION

A photograph and schematic of the calibration configuration are shown in Fig. 6. The rotating assembly consisted of a 19.38-in.-diam

cylindrical can supported from a flexure-mounted cradle by forward and aft bearing assemblies. A threaded steel retainer rod was placed through the can in an axial plane located 56 in. downstream of the upstream transverse load column. The distance between the transverse load columns was 84 in. The center of gravity of the symmetrical rod was positioned on the spin axis to within ±0.001 in.

Two stainless steel solid cylinders, threaded through their centerlines, were used to provide the specified unbalance. The cylinders weighed 10.043 and 5.020 lb_m and were threaded to the rod at varying radial locations to provide different levels of imparted unbalance.

An axial force of constant magnitude was applied to the thrust cradle by means of a deadweight acting through a bell crank lever mechanism to provide cradle force interaction effects.

3.2 INSTRUMENTATION

Instrumentation was provided to measure horizontal forces directed perpendicular to the spin axis at two axial locations. Double-bridge, strain-gage-type load cells having a range from 0 to 200 lb_f were employed. The angular position and rotational speed of the spin rig were determined by a magnetic pickup which provided a pulse output when screw pegs (Fig. 6b) passed the pickup face. The pegs were positioned angularly at 10-deg increments on the rotating assembly.

The d-c output signals from the force measuring load cells were amplified and recorded on a frequency modulated (FM) magnetic tape recording system. The pulse outputs from the rotational speed and angular position magnetic pickup were displayed on a photographically recording, galvanometer-type oscillograph which recorded at a paper speed of 16 in./sec.

After a calibration run, the FM recorded side load data were rerecorded on magnetic tape through electronic low pass filters in series with a multi-input, analog-to-digital converter. The filters were used to attenuate all frequencies (resulting from system vibration) greater than the rotational speed. Playback of this tape to an IBM 7074 computer provided a printed tabulation of force at 0.01-sec time increments. The angle at which the measured force maximized was determined from the filtered transverse force data and spin rig angular position pulses (Fig. 7) displayed on an oscillograph recorder. Details of the filtering technique are discussed in the Appendix.

3.3 PROCEDURE

After the cylindrical can and eccentric mass retainer rod were installed in the spin fixture, the rotating assembly was balanced to within 3.5 in.-lb_m. The total centrifugal force produced by the remaining 3.5 in.-lb_m unbalance was 1.0 lb_f at a rotational speed of 100 rpm. The calibration mass was then threaded to the retainer rod and locked at a radial position which would provide the desired level of imparted unbalance. The radius at which the mass was located was determined within 0.002 in. through precision measurement of the distance between the machined end of the retainer rod and the center of the calibration mass. The final level of unbalance which was used to determine the calculated centrifugal force was obtained by vectorially adding the measured residual system unbalance (3.5 in.-lb_m) and that calculated for the eccentric calibration mass. The force measuring load cells were then electrically calibrated, and a thrust simulating axial force of 4800 lb_f was applied. The rotating assembly was spun up, and data were recorded at nominal rotational speeds of 30, 140, 250, 190, and 80 rpm. Data were obtained at corrected unbalance levels of 54.65, 92.15, and 148.52 in.-lb_m with the facility equipment (which is normally used to provide high altitude pressure simulation) inoperative. Since this equipment would provide an additional energy source for exciting the system resonant frequencies, a series of spin-ups was accomplished with 92.15 in.-lb_m unbalance at a pressure altitude of approximately 100,000 ft to determine if higher amplitude extraneous vibrations could be effectively filtered from the calibration data.

A post-calibration check was made to verify that the magnitude and angular position of the residual system unbalance had not varied.

3.4 RESULTS

Calibration data were obtained at varying rotational speeds for nominal levels of unbalance of 50, 100, and 150 in.-lb_m and with a 4800-lb_f thrust simulating axial load applied to the flexure-mounted cradle. All data were obtained with the calibration (unbalance) force applied at an axial position 56 in. aft of the upstream transverse restraining column. This placement of the calibration force would theoretically provide in-phase sinusoidal variations in F_u and F_d with the magnitude of F_d being twice that of F_u. Data were also obtained with the test chamber evacuated to a pressure altitude of approximately 100,000 ft at the 100 in.-lb_m unbalance condition to determine the effect of higher vibration levels (from facility equipment) on data filtering capability.

The analog variation in measured transverse forces for a typical rotational speed (140 rpm) during the altitude run is presented in Fig. 7a. The high noise-to-signal ratio (~5 to 10) clearly indicates the necessity for data filtering. The data presented in Fig. 7b were obtained by re-recording the data shown in Fig. 7a through a low pass electronic filter. Filter calibrations indicated that filtering had no appreciable effect on data accuracy. A complete description of the filtering technique and data reduction methods is presented in the Appendix.

3.4.1 Comparison of Measured and Calculated Force Data

The measured total side force is presented in Fig. 8 as a function of rotational speed for three levels of forced unbalance. The calculated centrifugal force is also shown for comparison. It can be seen that the difference between the measured and calculated centrifugal force increased with rotational speed for all three unbalance conditions.

The ratio of measured to calculated centrifugal force is presented as a function of rotational speed in Fig. 9. The high departures of measured force from calculated centrifugal force at a rotational speed of 30 rpm occur because of the large effect that small force variations have on the force ratio at this condition. For example, the 15.5-percent deviation shown for 100 in.-lb_m unbalance at 30 rpm represents a measured force only 0.5 lb_f greater than the 3.23-lb_f calculated centrifugal force. The trend of increasing ratio of measured-to-calculated centrifugal force with rotational speed in Fig. 9 is the result of the dynamic effect of free vibrations acting in combination with forced vibration. The equations describing this dynamic effect are developed and discussed for a single-degree-of-freedom forced vibration system in Ref. 2, where the ratio of the measured to disturbing (centrifugal) force magnitude is termed the magnification factor. The magnification factor is proportional to the system natural frequency and damping ratio and to the frequency of the disturbing force. However, the effect of damping ratio on the magnification factor is small in the region where the impressed frequency is much less (~one-fourth) than the natural frequency. The curve shown in Fig. 9 represents the calculated variation in the magnification factor with rotational speed for a single-degree-of-freedom forced vibration system with a resonant frequency equivalent to that determined for the calibration configuration (12 cps) and with zero damping. The ratio of measured to centrifugal force clearly follows the theoretical variation of the magnification factor.

The difference between the actual and measured transverse force angular positions is presented in Fig. 10 as a function of rotational speed

for the 50 in.-lb_m unbalance condition. The measured angular position lagged the actual by an amount which increased with rotational speed to a value of 13 deg at 240 rpm. The angular difference results from the forced vibration angular phase lag (Ref. 2), which is associated with the previously discussed magnification factor. The three curves shown in Fig. 10 represent the theoretical variation in the forced vibration phase lag angle for a system having a natural frequency of 12 cps with varying damping ratios. Damping ratio measurements on systems comparable to that used during the calibration indicate that the damping ratio could be expected to be in the range of from 0.1 to 0.3. The phase lag measurements presented in Fig. 10 indicate the damping ratio to be approximately 0.2 with a scatter of ±5 deg, which is the smallest angular increment which can be accurately resolved from the 10-deg increment angular position pulses. The angular position was also determined within 5 deg during a more recent calibration where total nominal transverse forces of 2, 4, 6, 8, and 10 lb_f were produced at 100 rpm.

The variation in the ratio of the measured downstream to measured total force is presented in Fig. 11 as a function of force magnitude. This parameter is of significance during a motor firing since the apportionment of the total transverse force between the two axial measuring stations determines the axial position at which the motor misaligned thrust vector either intersects or is nearest the motor axial centerline (or spin axis). For the force calibration reported herein, the eccentrically mounted calibration mass was placed at an axial location, which should distribute the centrifugal force so that two-thirds of the total measured force is applied to the downstream transverse restraining column. It can be seen in Fig. 11 that the ratio ranged from 0.667 to 0.696 for all total force magnitudes greater than 10 lb_f. As previously discussed, the scatter shown for force levels less than 5 lb_f is the result of the large effect which small force deviations have at this operating level. Also presented in Fig. 11 is a scale which shows the indicated displacement of the calibration force (as determined from the force distribution) from the true axial position at which it was placed. The force distribution correctly indicated the axial placement of the calibration force within 3 in. for force levels greater than 10 lb_f.

3.4.2 Estimated Accuracy of Nonaxial Force Measurement

The calculated centrifugal force was corrected for the theoretical magnification factor previously discussed, and the subsequent parameter, F_{pred}, is used as a basis for comparison with measured forces. The difference between measured and predicted force is presented in Fig. 12 as a function of the magnitude of predicted force. Also shown are the respective upper and lower limits of the individual cyclic measurements,

which were averaged to obtain the points presented. It can be seen in Fig. 12 that the force difference varied about zero in a random manner. No trend in the force difference with level of unbalance or rotational speed is evident. In addition, no apparent effects from the additional background vibration imparted by equipment required for altitude simulation were observed. In general, average measured total side force was within 5 percent of the predicted force for all force levels greater than 10 lb_f. The difference between measured and predicted force was less than 0.5 lb_f at operating force levels less than 10 lb_f.

SECTION IV
NONAXIAL FORCE MEASUREMENT RESULTS DURING A MOTOR FIRING

The ability to measure small nonaxial forces using the spin technique was demonstrated during two recent motor firings in Propulsion Engine Test Cell (T-3) conducted at rotational speeds of 100 and 200 rpm. The data are presented to illustrate the nature of transverse force results which might be expected from a motor firing.

The variations in the upstream and downstream force measurements during the 100- and 200-rpm firings are shown in Figs. 13a and b, respectively. The data presented include corrections which were applied to account for the forced vibration magnification factor, electronic filter effects, and system unbalance forces. The unbalance correction was applied by assuming that the centrifugal force varied linearly with time from the pre- to the post-fire, steady-state conditions. Vector angular locations where the force magnitude is less than 0.5 lb_f are not shown (see Fig. 13a) since the angular data lose their significance as the vector magnitude approaches zero.

The magnitudes of the forces measured at the upstream and downstream stations during the 100-rpm firing were always less than 4.0 lb_f. The upstream force was less than 0.5 lb_f except during the period from 14.9 to 22.7 sec, during which the phase variance between the upstream and downstream force measurements ranged from 50 to 160 deg.

The magnitude of the downstream force measured during the 200-rpm firing ranged, primarily, from 6 to 18 lb_f. The upstream force magnitude remained around 2 lb_f throughout the firing. The phase difference between the upstream and downstream force vectors varied from approximately 60 deg at the start of the firing to approximately 120 deg at the end of the firing.

The fact that the upstream and downstream forces were out of phase throughout the entire burn time of the 200-rpm firing and during the period from 14.9 to 22.7 sec for the 100-rpm firing indicated the presence of coupling action.

After the upstream and downstream force vectors were determined, the vectors were translated to a common axial location (by the addition of a couple) and vectorially added to obtain a generalized nonaxial force system. The axial location chosen for the resultant force was determined such that the couple generated by translating the upstream and downstream force vectors was a minimum. The generalized force system, consisting of a single, radial force vector, a force axial location, and a couple, is equivalent to the original system consisting of the upstream and downstream force vectors. The system is unique in that the couple acts in a plane perpendicular to the radial force vector which minimizes the couple magnitude. Figures 14a and b present the resultant force system for the 100- and 200-rpm firings, respectively. The nonaxial force vector was generally located near the axial plane containing the motor exhaust nozzle for both firings. Since the downstream restraining column was also located in this region, the upstream measurements had only a small effect on the resultant vector magnitude and angular position.

SECTION V
CONCLUDING REMARKS

The results obtained from the dynamic transverse force calibration have demonstrated that nonaxial forces can be measured, using the spin technique, within 5 percent or 0.5 lb_f (whichever is larger) at rotational speeds to 250 rpm. The accuracy of measurement of the angular position at which the transverse force vector is directed depends on the force magnitude and the rotational speed of the system. The angular position can be determined within 5 deg at a nominal force level of 2 lb_f and a rotational speed of 100 rpm.

During a motor firing, additional inaccuracies may arise as a result of improper proration of the unbalance correction (normally assumed to vary linearly with time from pre- to post-fire) or from motor installation misalignment. Based on experience gained during previous motor firings, it is estimated that the magnitude of the unbalance correction could be expected to range from 3 to 5 lb_f depending upon the rotational speed during firing. It has also been demonstrated that a motor can be aligned so that the motor centerline is concentric with the spin axis within 0.0015 in. with little additional effort.

In summary, it is concluded that the spin technique for measuring nonaxial forces has significant advantages over the prevalent six-component stand method. This is particularly true for motors fired horizontally, where large corrections must be applied to the six-component stand pitch data to account for weight changes resulting from propellant consumption. In addition, a detailed knowledge of the six-component stand force interaction characteristics is essential for accurate data reduction, which necessitates costly stand interaction calibrations. The spin technique, however, does not include provisions for measurement of the roll component of the force system and does not provide for continuous measurements (with time) of the nonaxial force vector since the average value of the nonaxial force is determined only once during each motor revolution.

APPENDIX
FILTERING TECHNIQUE AND DATA REDUCTION METHODS

The spin technique for measurement of nonaxial forces from a solid-propellant rocket motor was evaluated by conducting a dynamic force calibration from which a comparison between the measured transverse force and calibration force was obtained. The calibration force was generated by an eccentrically mounted rotating mass which produced a calculable centrifugal force. The following discussion outlines the methods used to determine the measured and predicted (calibration) forces.

Measured Transverse Force

The output signals from the transverse force measuring load cells were composed of components produced by (1) the forces produced by free vibrations of the system and (2) the forces produced by the calibration mass. The free vibrations occurred at the system natural frequencies, whereas the frequency of the calibration force was equivalent to the rotational speed. The analog variation in the composite data signal for a typical calibration condition is shown below:

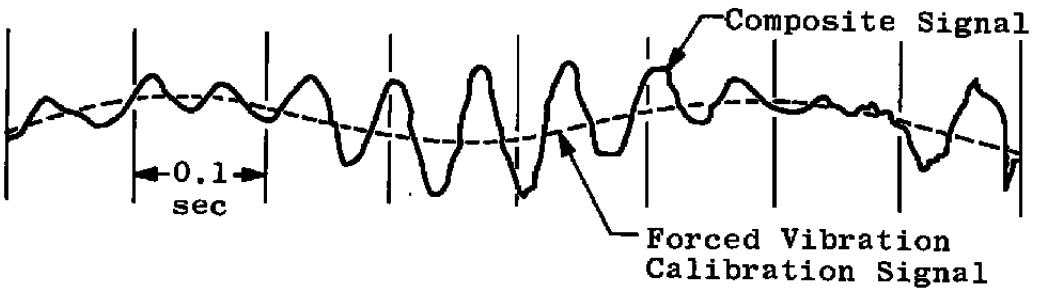

Since only the calibration force component of the composite signal is of interest, a method for separating this force from the free vibrations is essential for accurate force measurement. Extraction of the desired data from the described composite signal was accomplished with low pass electronic filters (one for the upstream signal and one for the downstream signal) which had the capability of passing direct current electrical calibration signals and incorporated an adjustment whereby all frequencies above a given frequency setting were attenuated at a rate of approximately 13 decibels per octave. In addition, however, the filters impart an angular phase lag (ϕ_f) between the input and output signals. Typical filter

amplitude attenuation and angular phase lag characteristics are shown below for some selected filter settings:

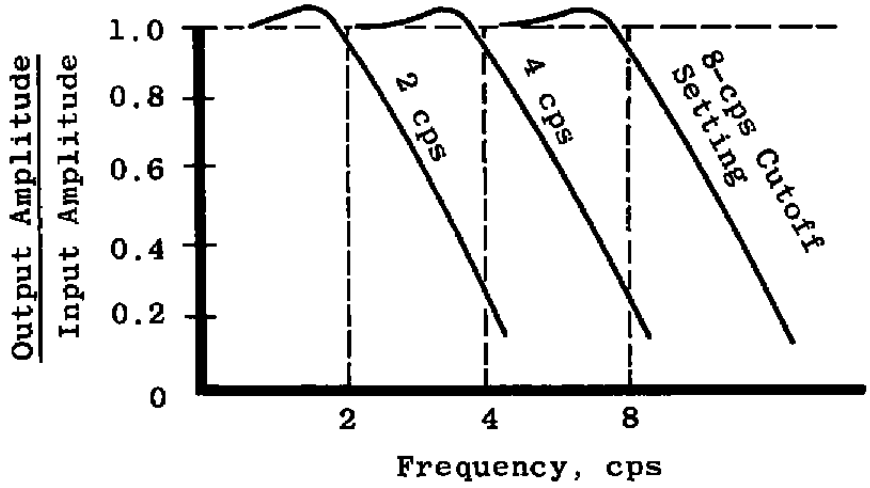

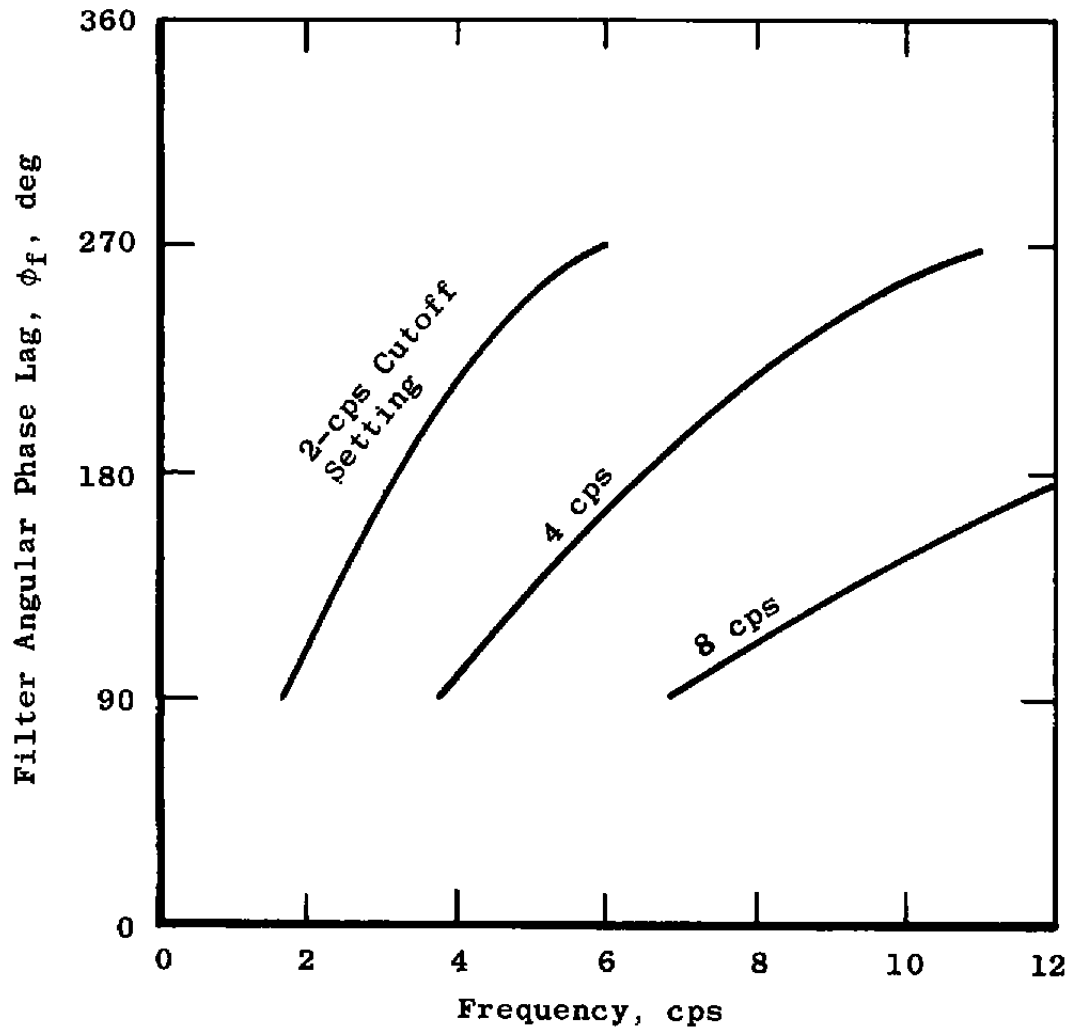

The calibration signal was extracted by re-recording the composite signals (upstream and downstream) through the low pass filters on an oscillograph and on magnetic tape recorders. The angular phase lag and amplitude effects of the filters on the data signals were determined through use of an electronic oscillator. The oscillator provided a signal at a frequency equivalent to the rotational speed which was transmitted to the filters. The filter input and output signals from the oscillator were recorded and compared to determine filter effects.

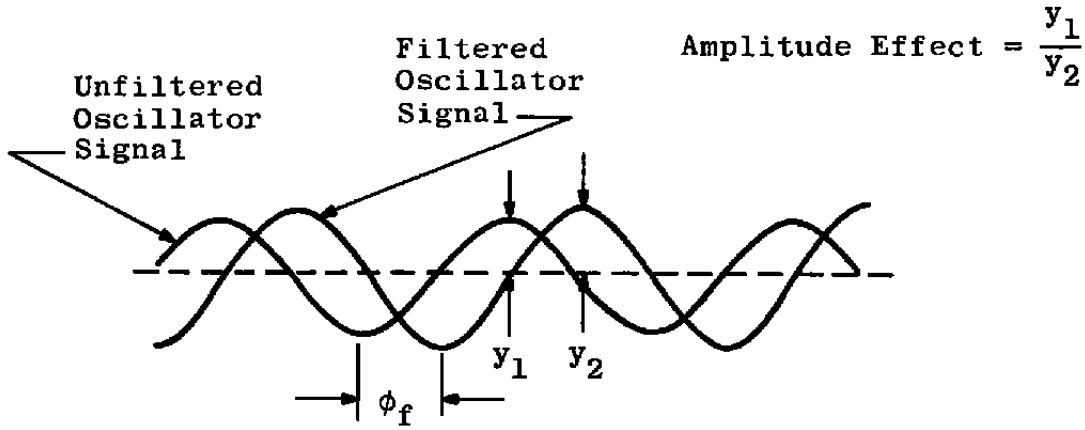

The angular phase lag was determined from the analog display on oscillograph. The amplitude effect (less than 1 percent) was determined from the digitized magnetic tape data.

The magnitude of the transverse force measured on the upstream and downstream load cells was determined by taking one-half of the algebraic difference between the maximum and minimum force values for each cycle of rotation (see Fig. 7b of the text). The upstream and downstream calibration force measurements were added to obtain the total transverse force since their cyclic variations were always in phase.

Predicted Force

The predicted force for each calibration condition is dependent on the system residual unbalance force, the imparted unbalance force, and the forced vibration magnification factor. The magnification factor is dependent on the system dynamic characteristics (Ref. 2) and is defined for a single-degree-of-freedom, second-order system by the following equation:

$$MF = \frac{1}{\sqrt{\left[1 - \left(\frac{\omega}{\omega_n}\right)^2\right]^2 + \left[2\zeta \frac{\omega}{\omega_n}\right]^2}}$$

where:

MF = magnification factor

ω = rotational frequency

ω_n = natural frequency

ζ = damping factor

The natural frequency was determined from wave analysis of data obtained from the calibration configuration to be 12 cps. The damping ratio was considered zero since its effect on the magnification factor is negligible in the region where the impressed frequency is much less than the natural frequency.

The residual unbalance was 3.5 in.-lb_m, as determined from forces measured at varying rotational speeds with no imparted unbalance.

$$(mr)_{res} = \frac{F}{\omega^2 (MF)}$$

The final unbalance force was obtained by vectorial addition of the residual and imparted unbalance. The final predicted calibration force used for data comparison was obtained from the following equation:

$$F_{pred} = (MF)\,\omega^2 \left[(mr)_{res} \mapsto (mr)_{imp}\right]$$

REFERENCES

1. Test Facilities Handbook, (5th Edition). "Rocket Test Facility, Vol. 2." Arnold Engineering Development Center, July 1963.

2. Timoshenko, S. Vibration Problems in Engineering, (3rd Edition). D. Van Nostrand Company, Inc., New York, January 1955.

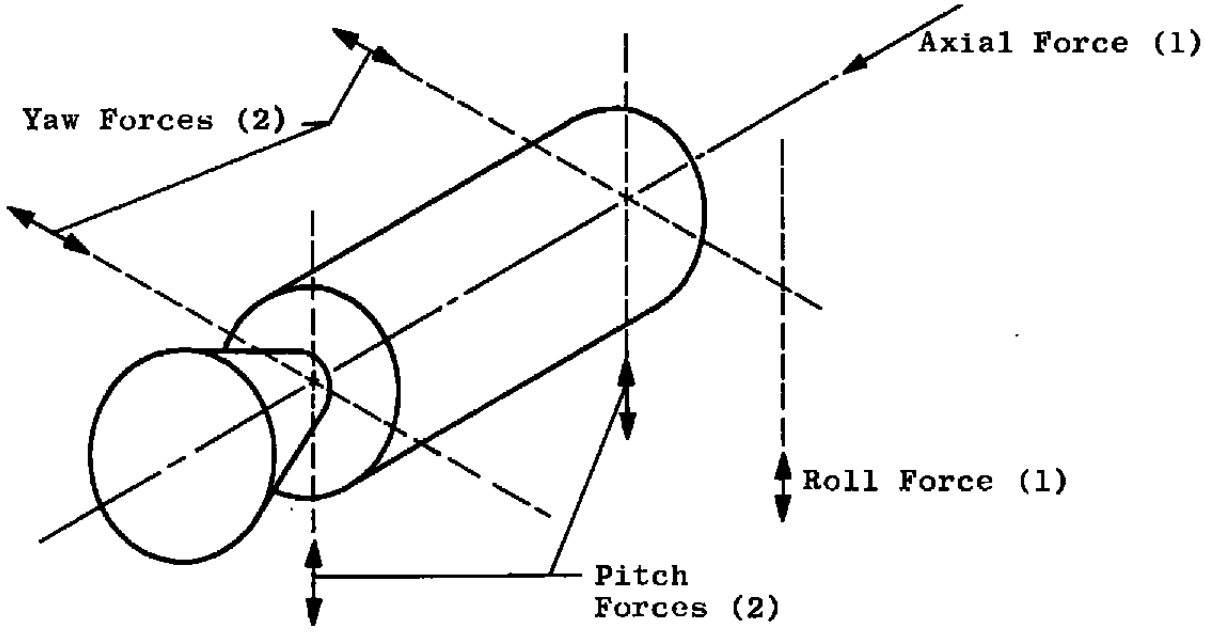

Fig. 1 Force Components Measured from Six-Component Stand

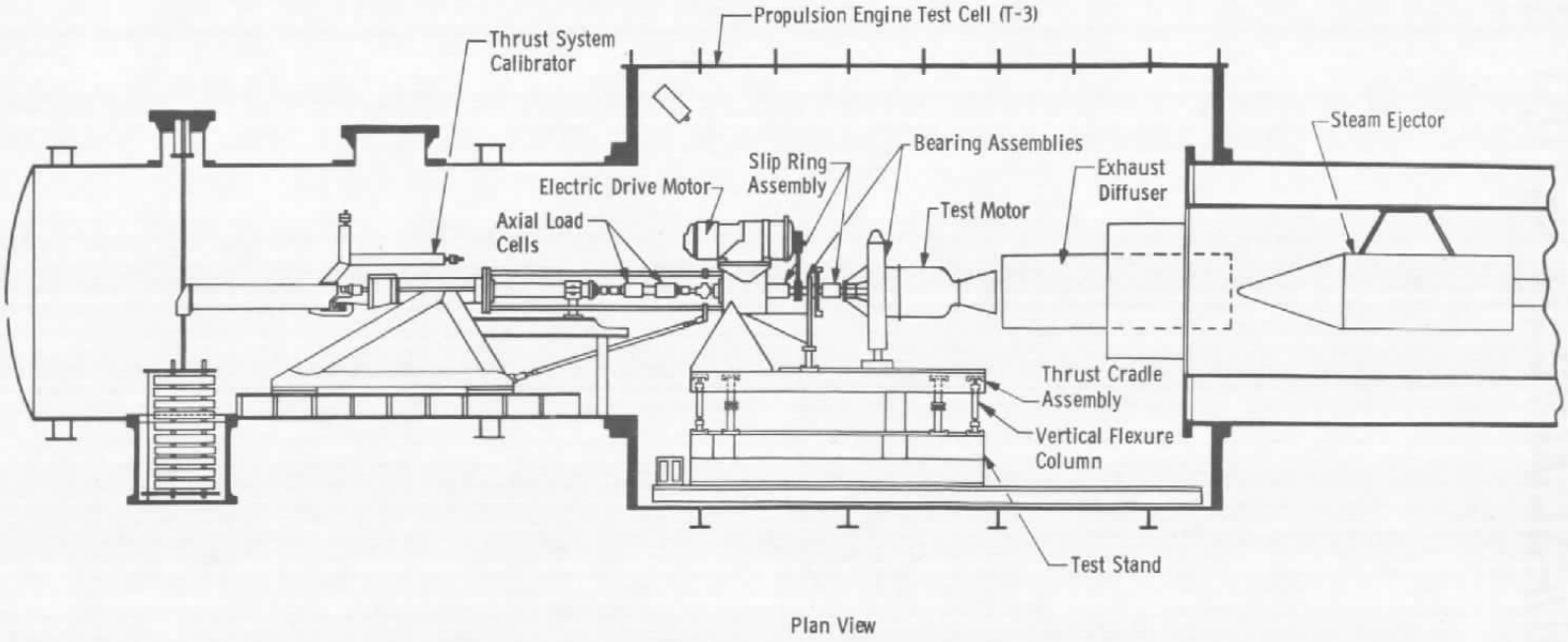

Fig. 2 Typical Test Configuration for Measurement of Nonaxial Forces Using the Spin Technique

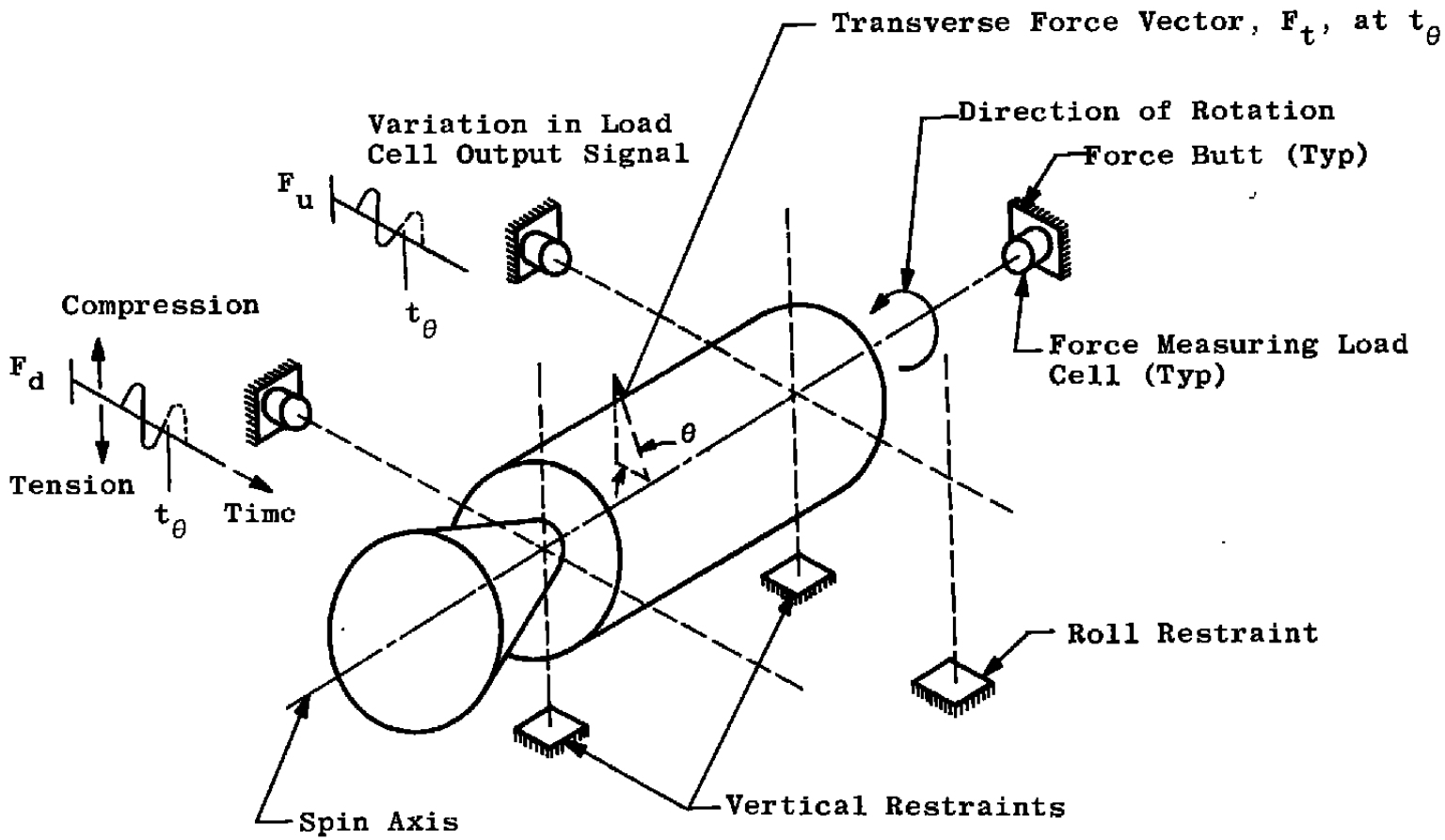

Fig. 3 Illustration of Spin Technique for Nonaxial Force Measurement

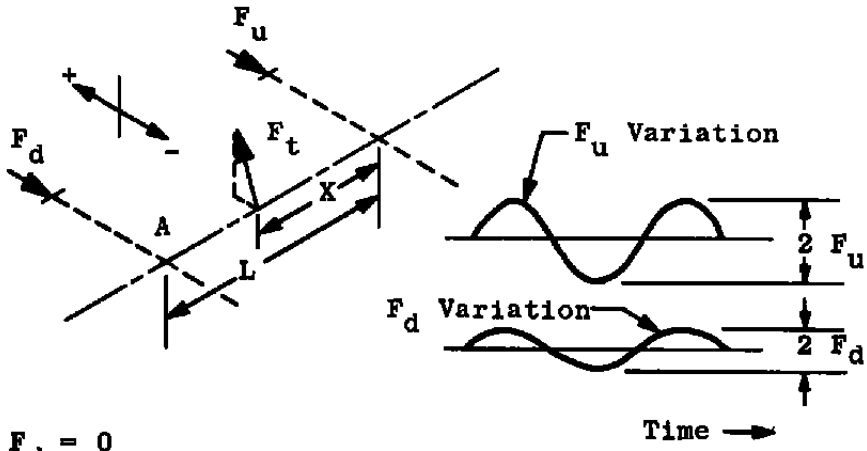

Magnitude of F_t;

$$\Sigma F = F_t - F_u - F_d = 0$$

$$F_t = F_u + F_d$$

Position of F_t;

$$\Sigma M_A^+ = (L - X)\, F_t - L\, F_u = 0$$

$$X = \frac{L\,(F_t - F_u)}{F_t}$$

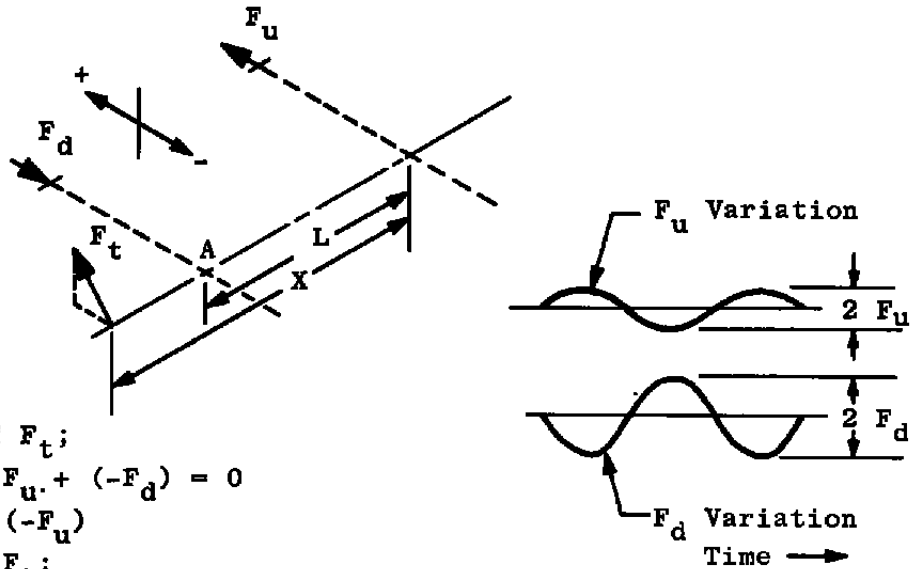

Magnitude of F_t;

$$\Sigma F = F_t + F_u + (-F_d) = 0$$

$$F_t = F_d + (-F_u)$$

Position of F_t;

$$\Sigma M_A^+ = L\, F_u - (X - L)\, F_t = 0$$

$$X = \frac{L\,(F_t + F_u)}{F_t}$$

Fig. 4 Schematic Showing Effect of Axial Location of Nonaxial Force on Phase Relationship of Measured Forces

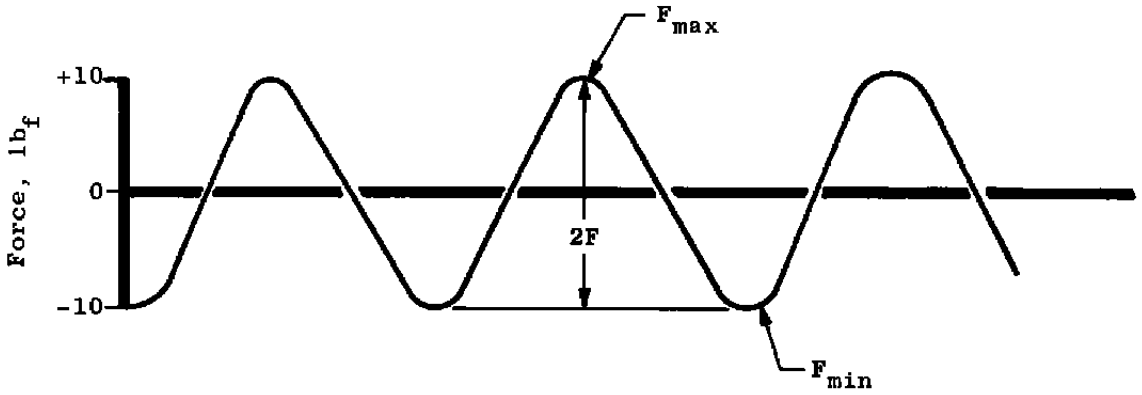

a. Without Thrust Stand Interaction

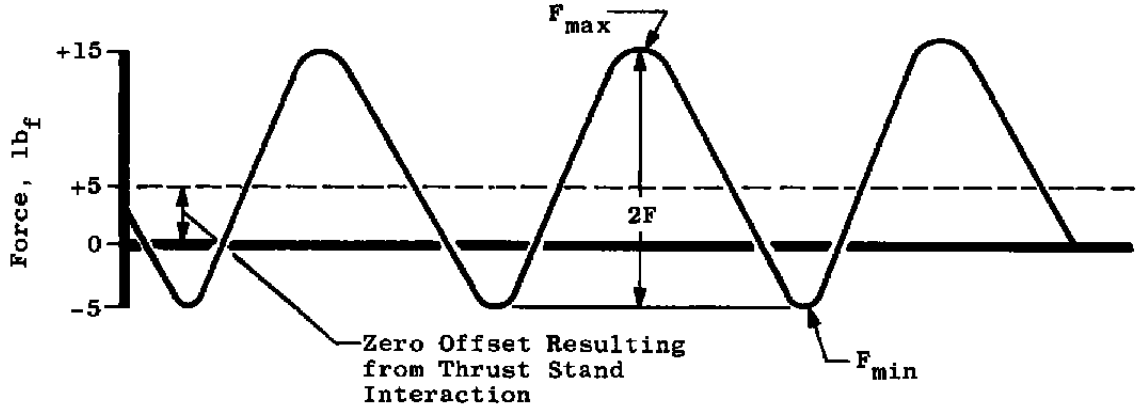

Example:

$$F = \frac{1}{2}\left[F_{max} - F_{min}\right]$$

$$= \frac{1}{2}\left[(+15) - (-5)\right] = 10.0$$

$$\text{Zero Offset} = \frac{1}{2}\left[F_{max} + F_{min}\right]$$

$$= \frac{1}{2}\left[(+15) + (-5)\right] = 5.0$$

b. With Thrust Stand Interaction

Fig. 5 Example of Measured Force Variation during Rotation of a Transverse Force Vector

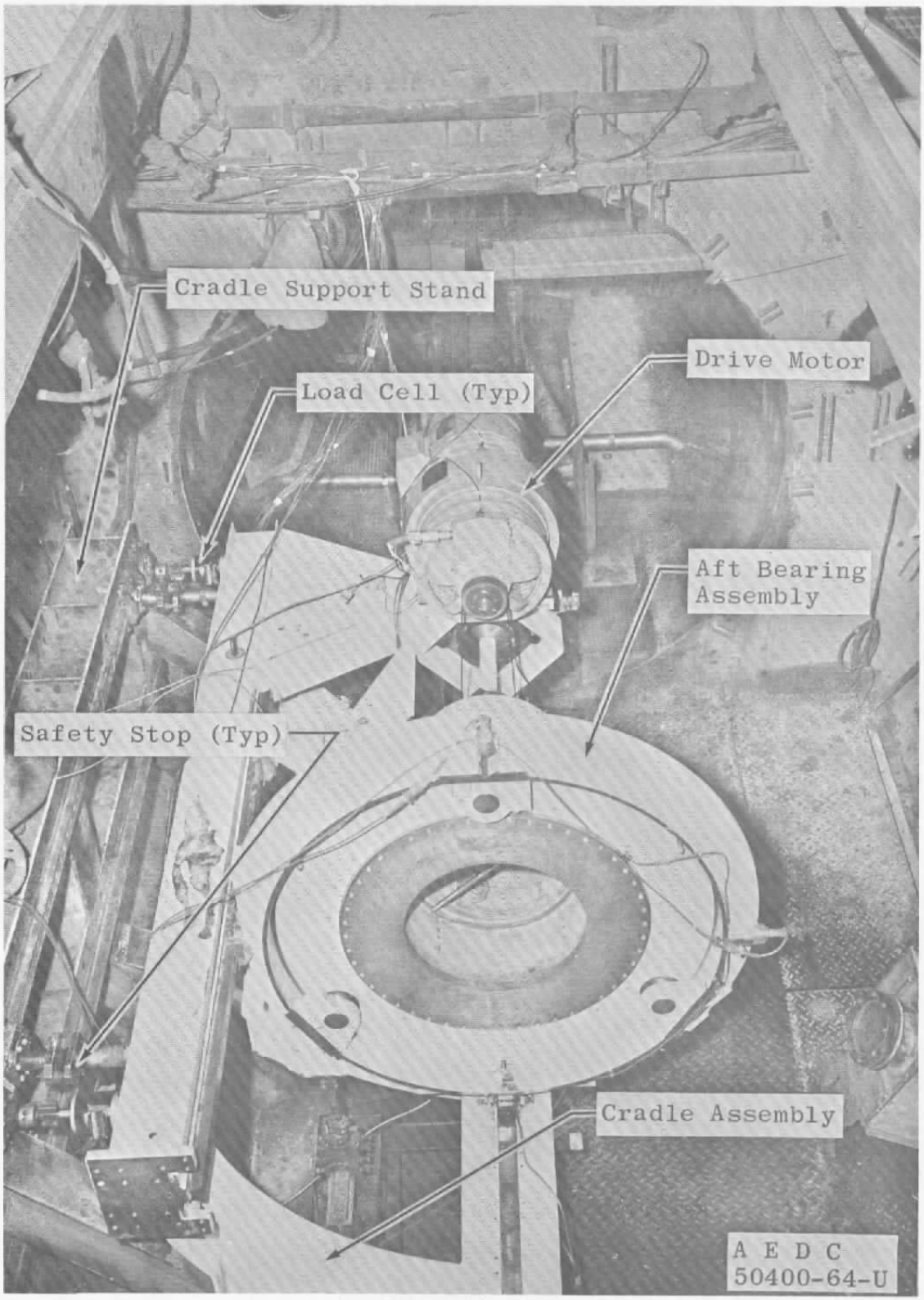

a. Top View, Looking Upstream

Fig. 6 Dynamic Transverse Force Calibration Configuration

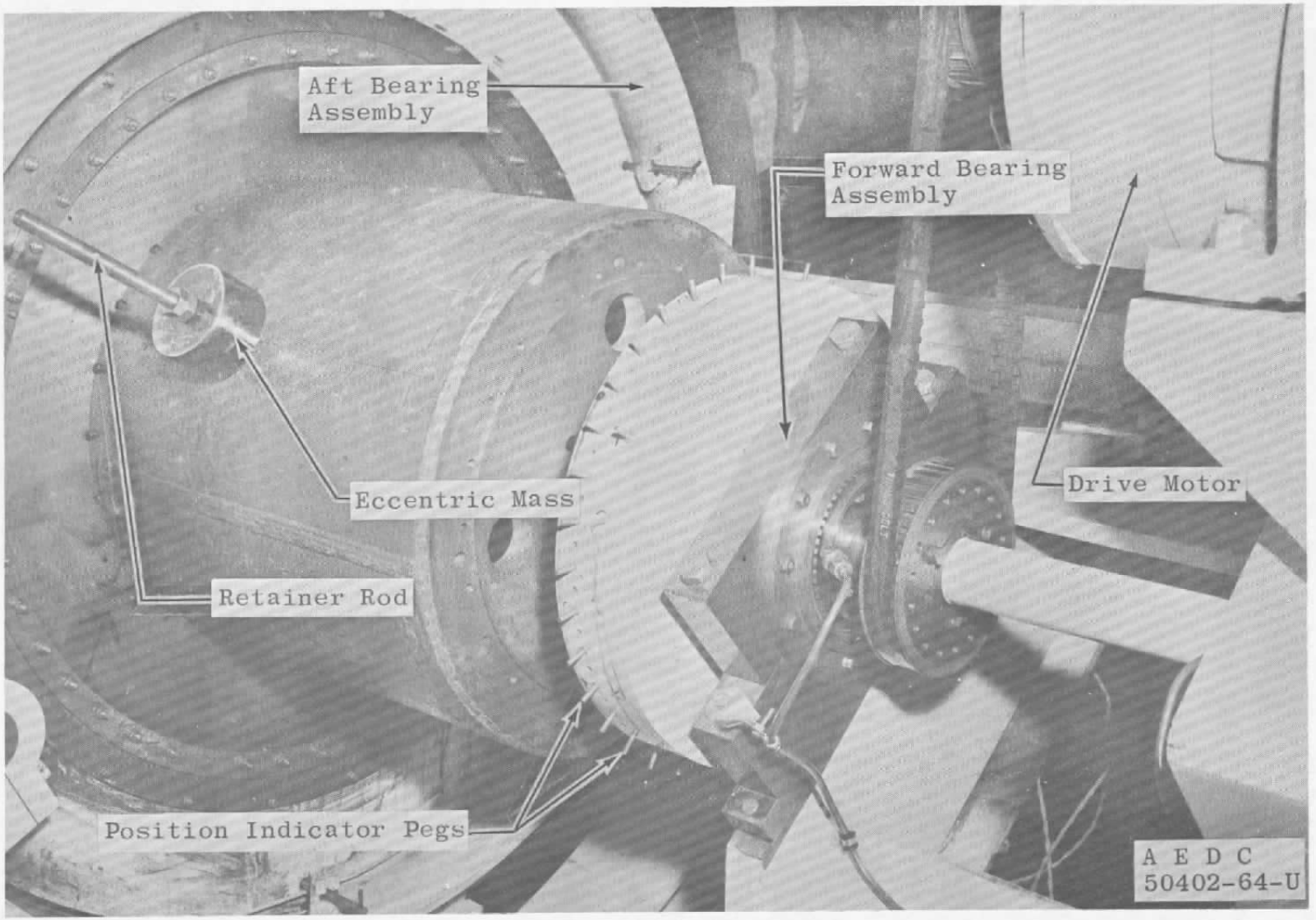

b. Side View, Showing Eccentric Mass

Fig. 6 Continued

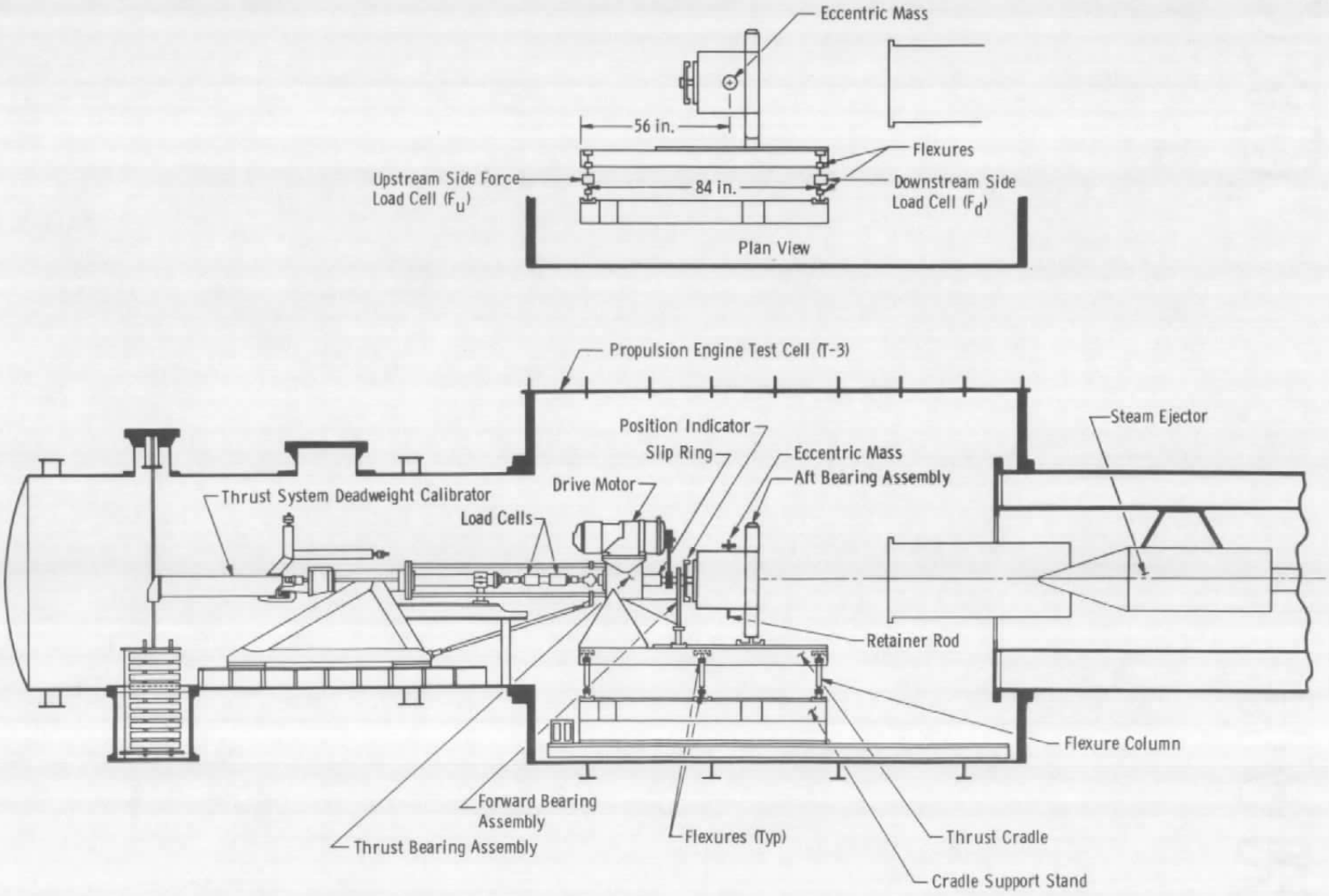

c. Schematic

Fig. 6 Concluded

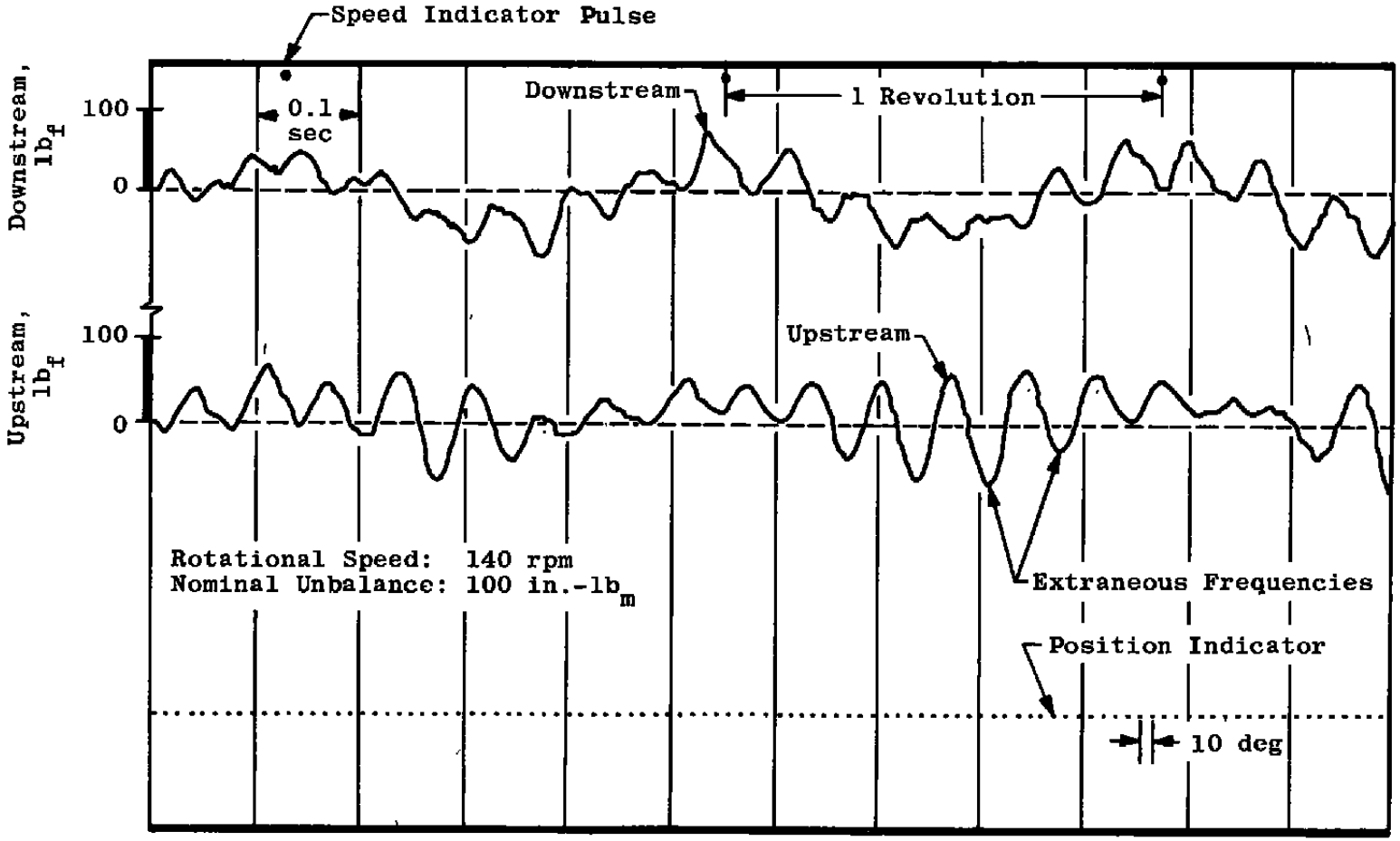

a. Unfiltered

Fig. 7 Typical Analog Trace of Variation in Upstream and Downstream Measured Force (Pressure Altitude = 100,000 ft)

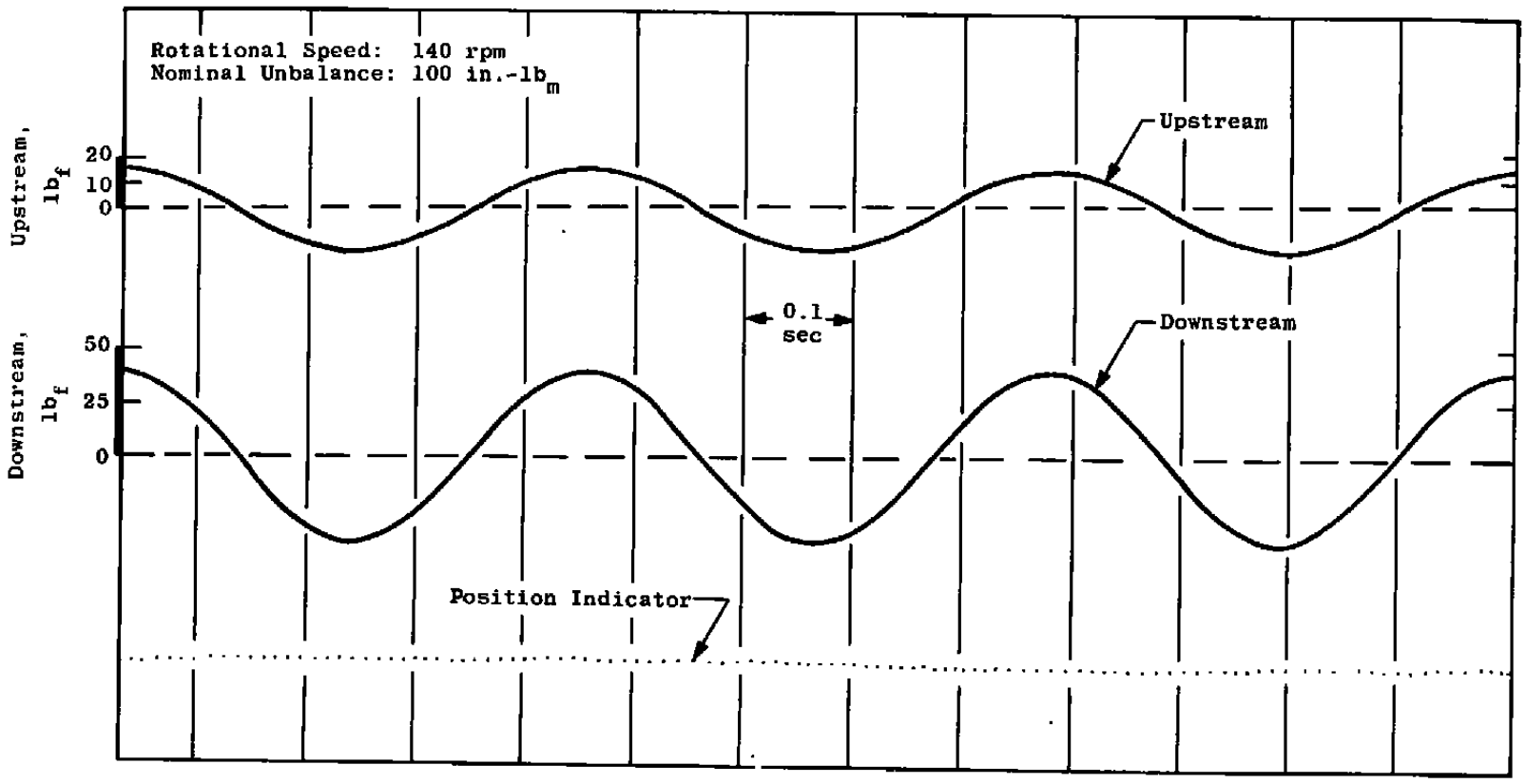

b. Filtered

Fig. 7 Concluded

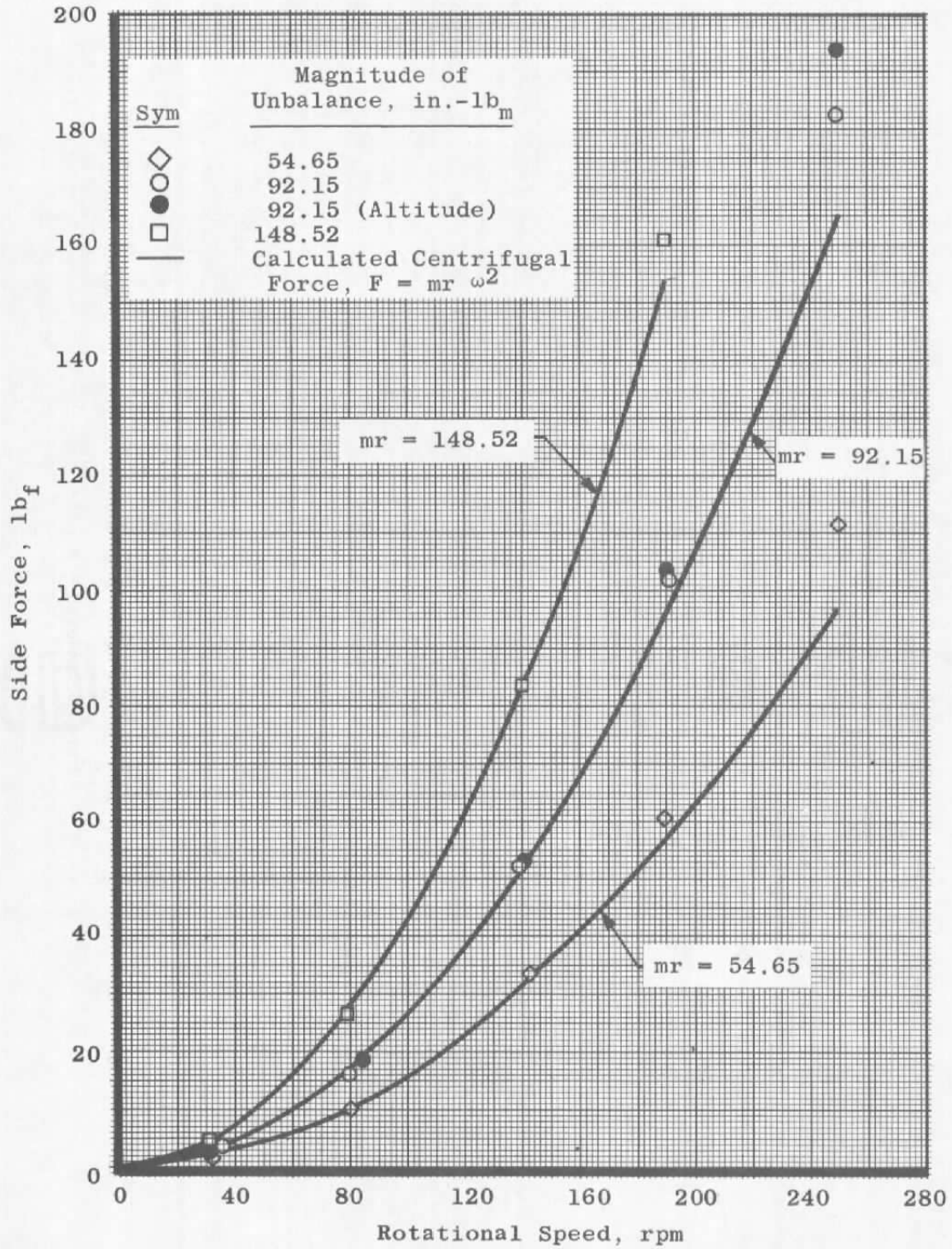

Fig. 8 Comparison of Measured and Calculated Centrifugal Force with Rotational Speed

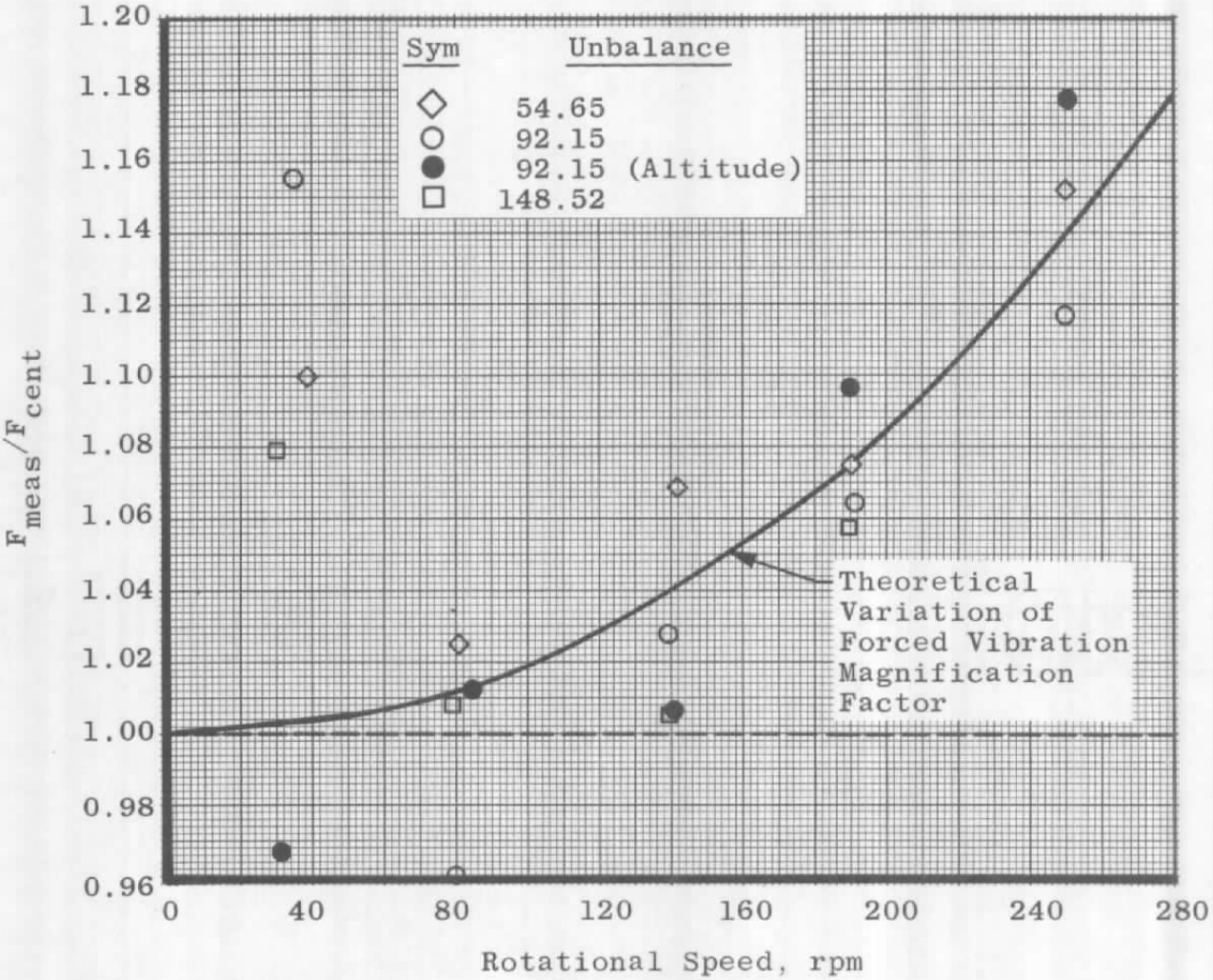

Fig. 9 Comparison of Ratio of Measured to Calculated Centrifugal Force with Theoretical Values

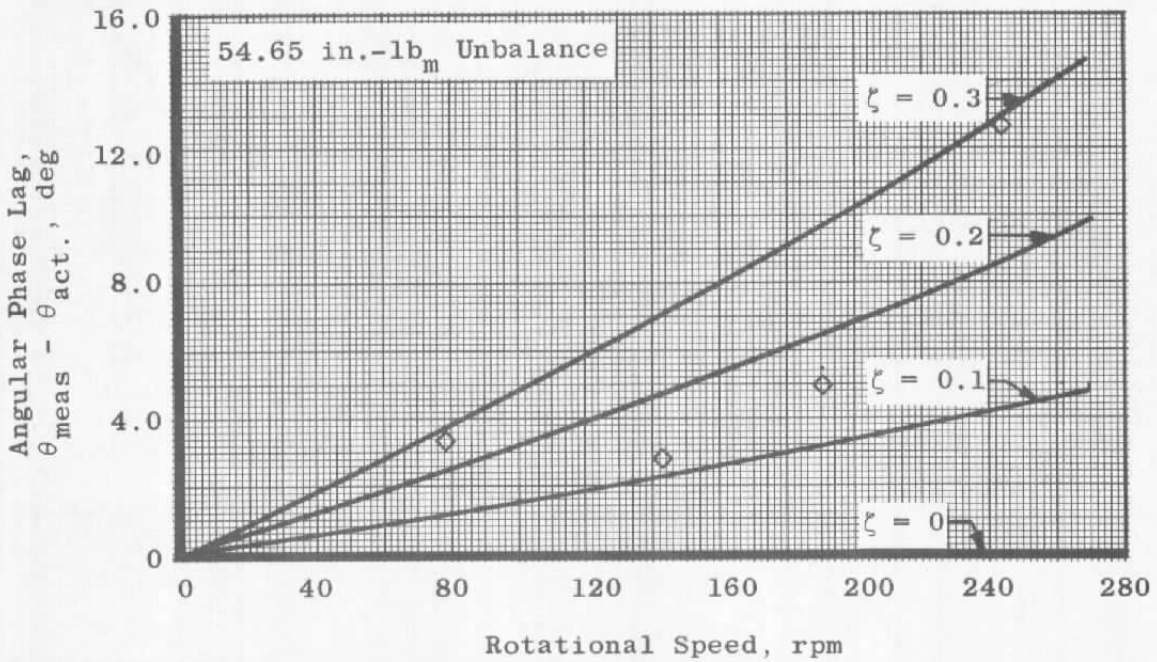

Fig. 10 Difference between Measured and Actual Angular Position of Transverse Force

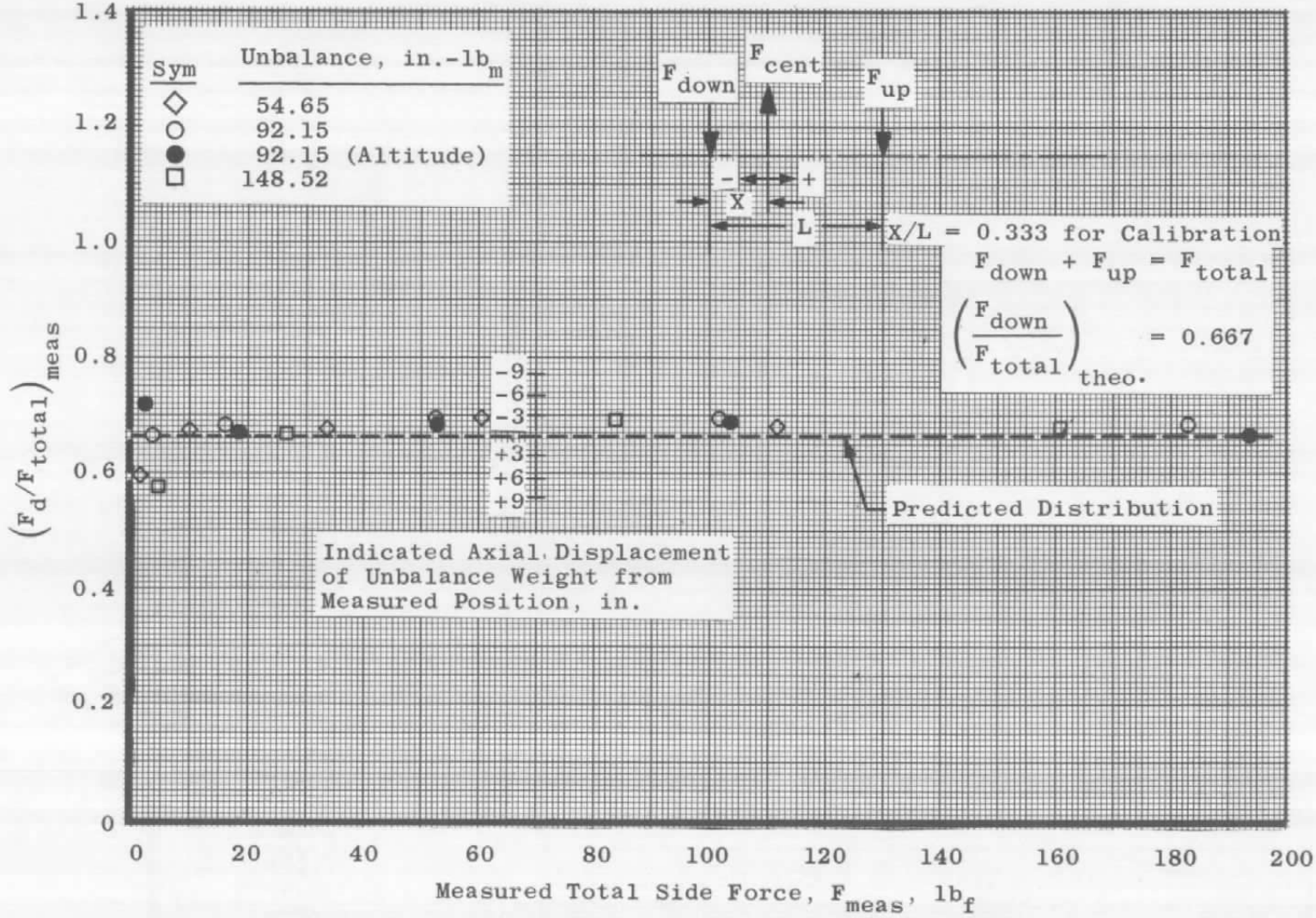

Fig. 11 Distribution of Measured Total Side Force between the Upstream and Downstream Transverse Restraining Columns

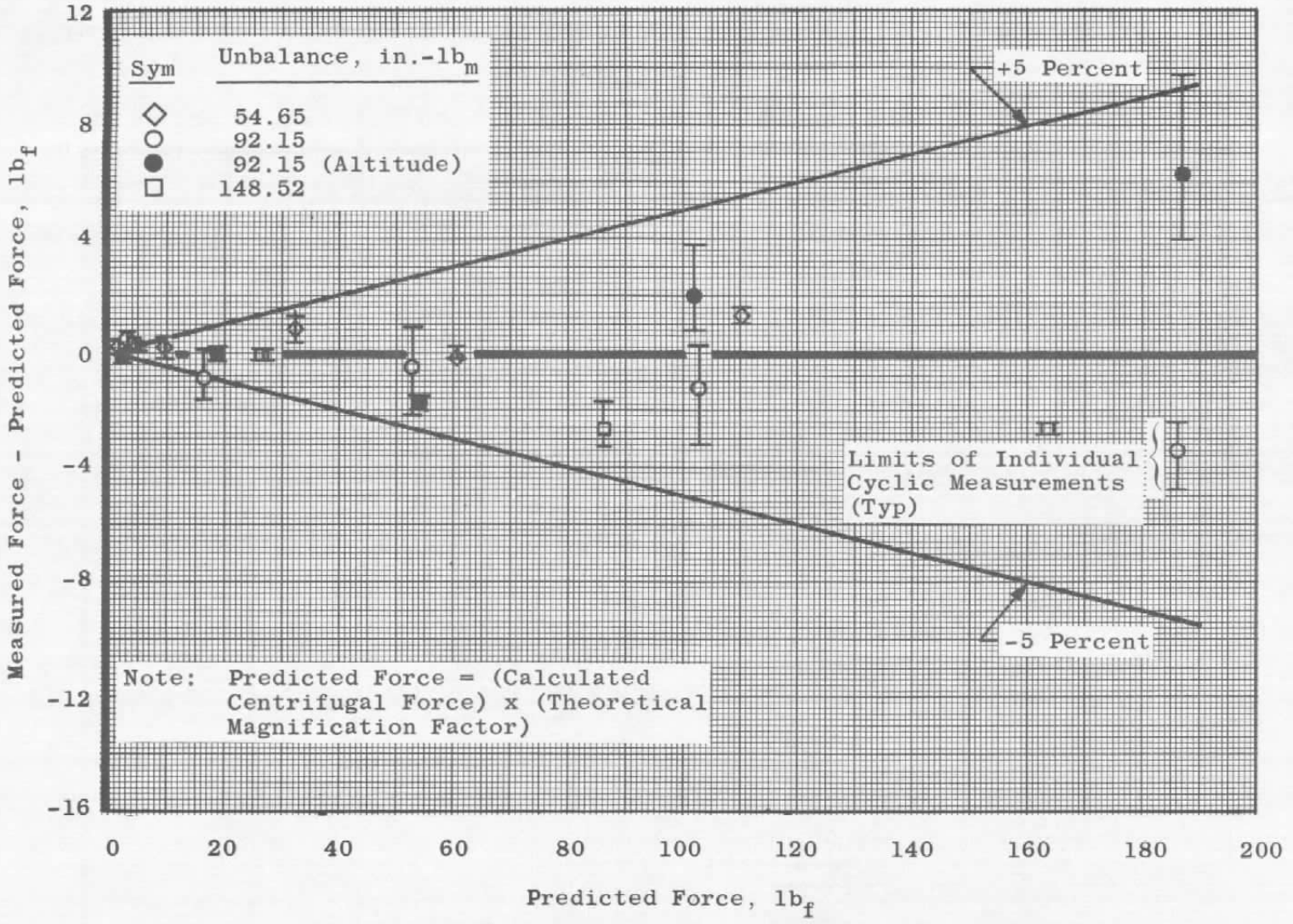

Fig. 12 Variation in Difference between Measured and Predicted Transverse Force with Predicted Force Magnitude

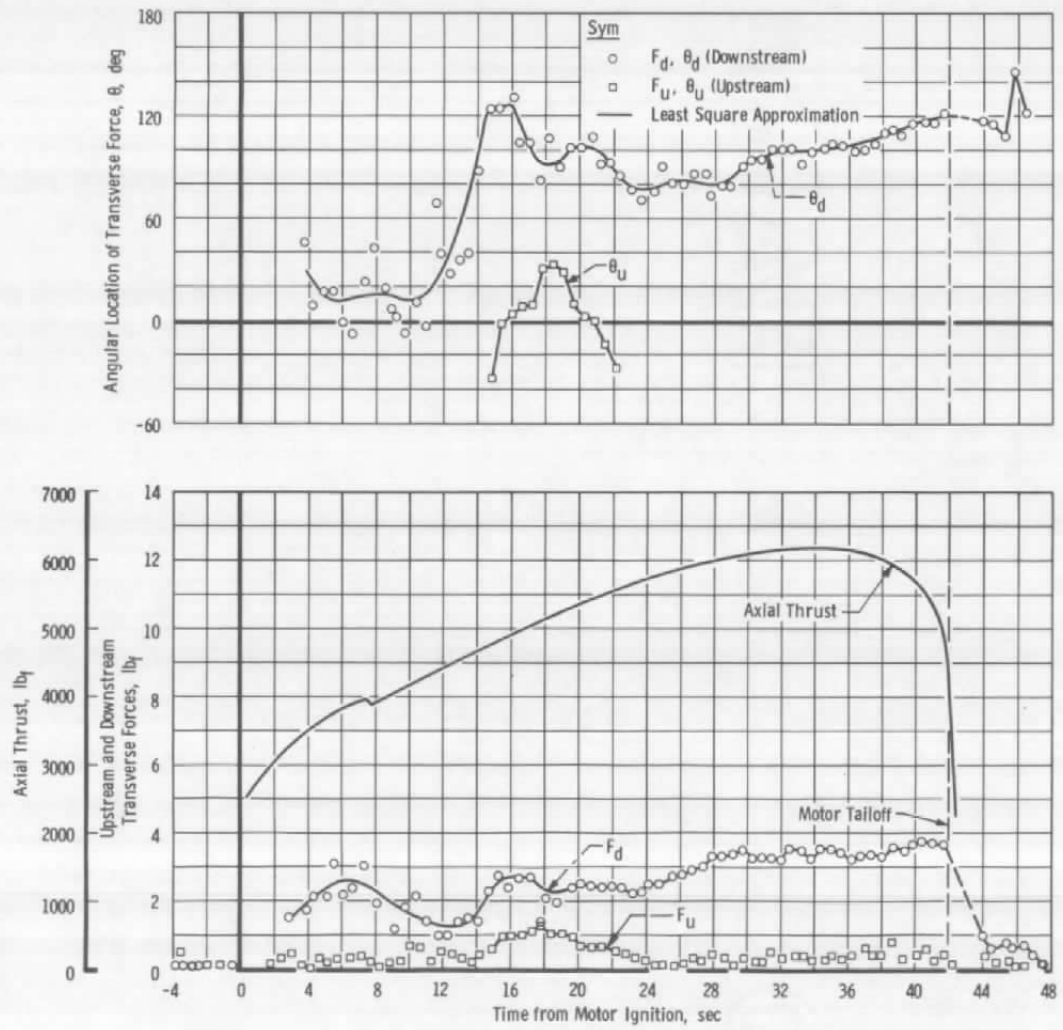

a. Rotational Speed, 100 rpm

Fig. 13 Force Measurements in the Upstream and Downstream Transverse Restraining Columns during Typical Motor Firings

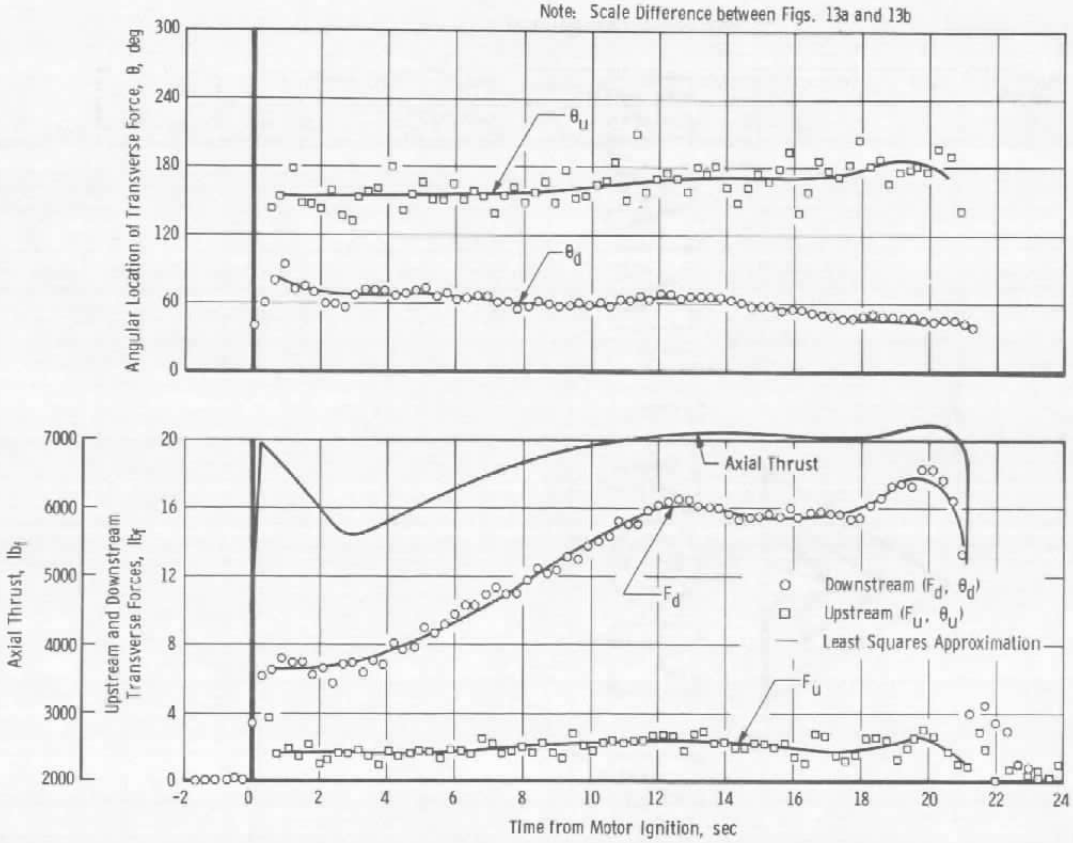

b. Rotational Speed, 200 rpm

Fig. 13 Concluded

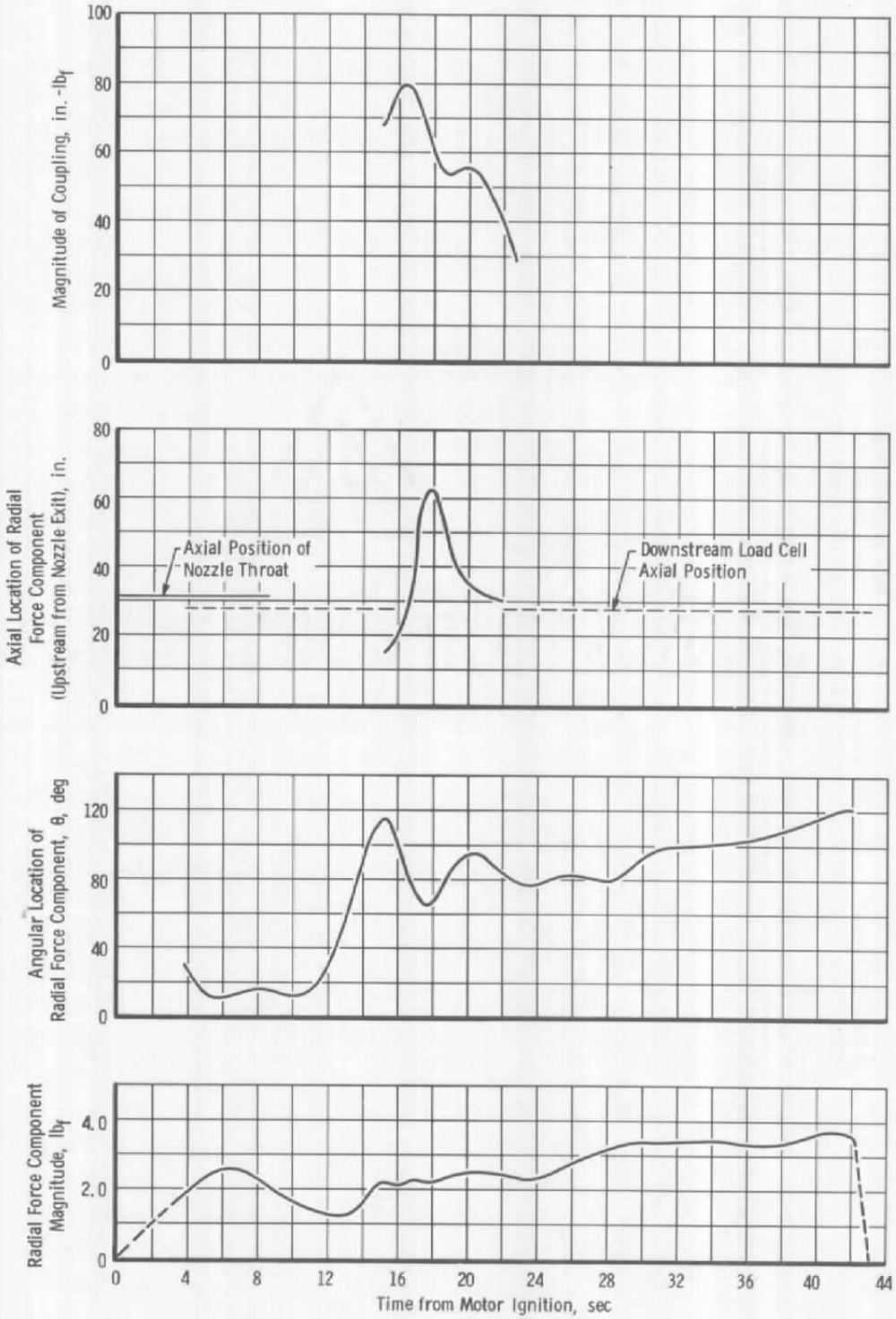

a. Rotational Speed, 100 rpm

Fig. 14 Generalized Presentation of Radial Force Components during Typical Motor Firings

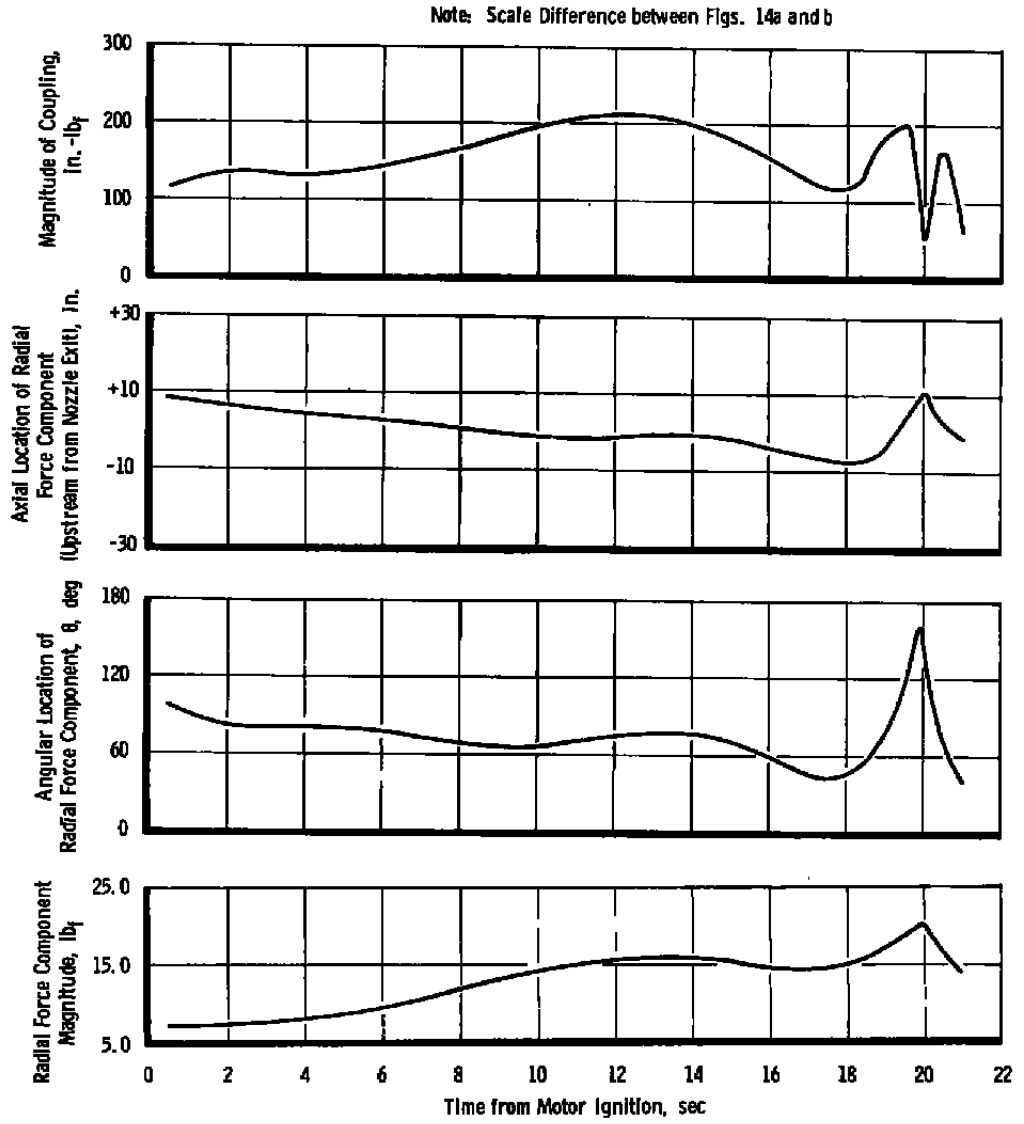

b. Rotational Speed, 200 rpm

Fig. 14 Concluded

DOCUMENT CONTROL DATA - R&D

(Security classification of title, body of abstract and indexing annotation must be entered when the overall report is classified)

1 ORIGINATING ACTIVITY (Corporate author) Arnold Engineering Development Center, ARO, Inc., Operating Contractor, Arnold Air Force Station, Tennessee	2a REPORT SECURITY CLASSIFICATION UNCLASSIFIED 2b GROUP N/A

3 REPORT TITLE

MEASUREMENT OF NONAXIAL FORCES PRODUCED BY SOLID-PROPELLANT ROCKET MOTORS USING A SPIN TECHNIQUE

4 DESCRIPTIVE NOTES (Type of report and inclusive dates)

N/A

5 AUTHOR(S) (Last name, first name, initial)

Nelius, M. A., and Harris, J. E., ARO, Inc.

6 REPORT DATE	7a. TOTAL NO. OF PAGES	7b. NO. OF REFS
November 1965	40	2

8a CONTRACT OR GRANT NO.	9a. ORIGINATOR'S REPORT NUMBER(S)
AF40(600)-1200 b Program Element 65402234	AEDC-TR-65-228
c d	9b. OTHER REPORT NO(S) (Any other numbers that may be assigned this report) N/A

10. AVAILABILITY/LIMITATION NOTICES

Qualified requesters may obtain copies of this report from DDC. DDC release to CFSTI and foreign announcement and distribution of this report are not authorized.

11. SUPPLEMENTARY NOTES	12. SPONSORING MILITARY ACTIVITY
N/A	Arnold Engineering Development Center, Air Force Systems Command, Arnold Air Force Station, Tennessee

13 ABSTRACT

This report introduces a technique for measurement of nonaxial forces produced by solid-propellant rocket motors which is independent of thrust stand interactions and motor weight variations. The technique consists of measuring the axial and two horizontal transverse forces (three components) while spinning the motor about its axial centerline. The accuracy of radial force measurement using the spin technique was established from a dynamic transverse force calibration which was accomplished in the presence of a 4800-lb_f, thrust-simulating axial load. It was determined that radial forces having magnitudes less than 10 lb_f could be determined within 0.5 lb_f and that radial forces greater than 10 lb_f could be determined within 5 percent at rotational speeds up to 250 rpm. The principle of the technique, its limitations, and advantages are discussed. Details of the dynamic transverse force calibrations and test results of nonaxial force measurements during motor firings are also presented.

DD FORM 1 JAN 64 1473

14 KEY WORDS	LINK A		LINK B		LINK C	
	ROLE	WT	ROLE	WT	ROLE	WT
rocket motors						
solid propellants						
nonaxial forces						
transverse forces						
measurements						
spin techniques						

INSTRUCTIONS

1. ORIGINATING ACTIVITY: Enter the name and address of the contractor, subcontractor, grantee, Department of Defense activity or other organization *(corporate author)* issuing the report.

2a. REPORT SECURITY CLASSIFICATION: Enter the overall security classification of the report. Indicate whether "Restricted Data" is included. Marking is to be in accordance with appropriate security regulations.

2b. GROUP: Automatic downgrading is specified in DoD Directive 5200.10 and Armed Forces Industrial Manual. Enter the group number. Also, when applicable, show that optional markings have been used for Group 3 and Group 4 as authorized.

3. REPORT TITLE: Enter the complete report title in all capital letters. Titles in all cases should be unclassified. If a meaningful title cannot be selected without classification, show title classification in all capitals in parenthesis immediately following the title.

4. DESCRIPTIVE NOTES: If appropriate, enter the type of report, e.g., interim, progress, summary, annual, or final. Give the inclusive dates when a specific reporting period is covered.

5. AUTHOR(S): Enter the name(s) of author(s) as shown on or in the report. Enter last name, first name, middle initial. If military, show rank and branch of service. The name of the principal author is an absolute minimum requirement.

6. REPORT DATE: Enter the date of the report as day, month, year, or month, year. If more than one date appears on the report, use date of publication.

7a. TOTAL NUMBER OF PAGES: The total page count should follow normal pagination procedures, i.e., enter the number of pages containing information.

7b. NUMBER OF REFERENCES: Enter the total number of references cited in the report.

8a. CONTRACT OR GRANT NUMBER: If appropriate, enter the applicable number of the contract or grant under which the report was written.

8b, 8c, & 8d. PROJECT NUMBER: Enter the appropriate military department identification, such as project number, subproject number, system numbers, task number, etc.

9a. ORIGINATOR'S REPORT NUMBER(S): Enter the official report number by which the document will be identified and controlled by the originating activity. This number must be unique to this report.

9b. OTHER REPORT NUMBER(S): If the report has been assigned any other report numbers *(either by the originator or by the sponsor)*, also enter this number(s).

10. AVAILABILITY/LIMITATION NOTICES: Enter any limitations on further dissemination of the report, other than those imposed by security classification, using standard statements such as:

(1) "Qualified requesters may obtain copies of this report from DDC."

(2) "Foreign announcement and dissemination of this report by DDC is not authorized."

(3) "U. S. Government agencies may obtain copies of this report directly from DDC. Other qualified DDC users shall request through _____."

(4) "U. S. military agencies may obtain copies of this report directly from DDC. Other qualified users shall request through _____."

(5) "All distribution of this report is controlled. Qualified DDC users shall request through _____."

If the report has been furnished to the Office of Technical Services, Department of Commerce, for sale to the public, indicate this fact and enter the price, if known.

11. SUPPLEMENTARY NOTES: Use for additional explanatory notes.

12. SPONSORING MILITARY ACTIVITY: Enter the name of the departmental project office or laboratory sponsoring *(paying for)* the research and development. Include address.

13 ABSTRACT: Enter an abstract giving a brief and factual summary of the document indicative of the report, even though it may also appear elsewhere in the body of the technical report. If additional space is required, a continuation sheet shall be attached.

It is highly desirable that the abstract of classified reports be unclassified. Each paragraph of the abstract shall end with an indication of the military security classification of the information in the paragraph, represented as *(TS), (S), (C), or (U)*

There is no limitation on the length of the abstract. However, the suggested length is from 150 to 225 words.

14. KEY WORDS: Key words are technically meaningful terms or short phrases that characterize a report and may be used as index entries for cataloging the report. Key words must be selected so that no security classification is required. Identifiers, such as equipment model designation, trade name, military project code name, geographic location, may be used as key words but will be followed by an indication of technical context. The assignment of links, rules, and weights is optional.

44-65

Some investigations on random lateral thrust with solid propellant rocket motors

W. Buschulte und K. Schadow

Deutsche Forschungsanstalt für Luft- und Raumfahrt e.V.
Insitut für Strahlantriebe
Trauen über Soltau/Hannover
GERMANY

Introduction

It is general practice to alter the direction of the flight-trajectory of missiles by lateral thrust produced by the propulsion device. These forces act vertically to the missile axis. Various means are known and applied to generate such lateral forces by the missile propulsion system.

Flight experiments with unguided missiles some time ago showed that random lateral forces must also be created by the rocket motor. Therefore we started a research program to clarify the origin, the effect and the influence of those lateral forces arising during motor firings. The propulsion units used were solid propellant rockets.

Although these side-forces are generally small compared to the axial thrust, they may bring loads onto the airframe of a missile, which cannot be neglected in all cases, especially if one thinks of larger missiles, where the structure is not so stiff as with small rockets. The investigations have been down with small rockets, but may related to larger units as well.

Subject of this paper will be to show some of the investigations performed and the basic results obtained.

Theoretical considerations on possible causes for lateral thrust

As disturbances of unknown nature are the origin of the unfavourable behaviour of the rocket motors, the explained problem cannot be attacked by theoretical-mathematical treatment up to this time. So an experimental-way-of-approach seemed to be the only possible treatment. To establish a working program various causes have been considered. Thereby four different groups have been found.

The first category is not included in our test program. It comprises the interaction of the motor jet with the free flow around the missile body. With unfavourable geometrical configurations lateral forces can be produced. But normally these configurations are axisymmetric, so that lateral thrust forces must not be expected.

The second group is characterized by working conditions, where the nozzle flow is not yet or no more fully developed, this preferably occurs during the ignition and the burn-out phase. When the pressure in the nozzle compared to the ambient pressure is too low, the flow separates off the nozzle wall and thus produces non-symmetric pressure distribution

at the nozzle wall and hence lateral forces. Various reports have been published concerning jet separation, so that the characteristics of it are quite well understood.

The third group of possible causes comprises those which do create lateral forces due to processes occuring within the supersonic (i.e. diverging) part of the thrust-nozzle. As too large diverging angles and undue surface roughness as possible causes are excluded, only thermodynamic or chemical phenomena which are non-symmetrically distributed across the nozzle cross-section are to be considered. Here one has to think of differences in recombination energies or velocities of combustion gases of unequal mixture-ratio or afterburning due to uncompleted combustion in the chamber.

The fourth group then comprises all phenomena occuring inside the combustion chamber and in the subsonic portion of the nozzle also influencing the flow downstream the nozzle throat. Besides those of thermochemical nature some causes due to aerodynamic character are conceiveable. From uneven combustion or by the configuration of the propellant block non-axisymmetric flow towards the expansion - nozzle may be induced and such produce uneven velocity - and pressure distribution in the whole nozzle flow.

3. Experimental investigations

Causes of the first group cannot be investigated by us because of lack of technical means. The causes of the second group are already well understood. Therefore we started a program aiming at the causes of groups three and four. They are very difficult to study, as that occur under conditions inside the combustion chamber and the nozzle, where measurements of the change of state in the gas flow are almost impossible to perform. First we tried to study the aerodynamic part of the possible causes and to find out, whether lateral forces are created upstream or downstream the nozzle throat.

3.1 The air-flow model for flow simulation

Figure 1 shows an air-flow model, which simulates the flow inside a rocket motor and through the nozzle. Compressed air was used as working gas. The pieces simulating the propellant charge and the nozzle contour can be exchanged by other profiles and contours.

The flow was visualized by the Schlieren-technique in the supersonic nozzle part. Mach waves are produced by thin wires of 0.05 mm diameter (Fig. 2b). The supersonic flow was visualized by a mixture of Al-powder and turpentine painted on one of the windows. The flow pattern then is visible by the ordering of Al-grains by the air-flow (Fig. 2a).

The chamber pressure, which the model-chamber is operated with, is in the range from 5 to 15 atmospheres.

Photographs as well as high-speed films were taken to resolve the development of the flow-pattern.

3.2 Three-component thrust rig for motor firings

For side-force measurements with rocket motors a three-component thrust rig

was built (Fig5). It allowed to measure axial thrust and the lateral forces in two planes being perpendicular to each other. Wires, attached to the motor near the nozzle lead to quartz-load cells, which are preloaded by weights being connected to the rocket motor again by a wire and over a wheel at the edge of the rig construction. During the experiments it was noticed, that the side-force measurement was influenced by heat conduction and radiation onto the load-cell and the cable, so that heavy insulation was applied to the cell and cable. In addition the load-cells are watercooled.

The minimum side-force, that can be resolved by this test rig, is in the order of five grams while the mean side-force values observed are in the order of several ten to several hundred grams. An influence of axial loads onto the side-force pickups was not observed as well as there is no interference between the two side-force pickups when load is applied to one of them only.

The rocket motor used developed a thrust in the order of 150 kg. Propellants burnt are double-base and composite powder. The double-base charges stem from the production line of a factory, while the composite charges have been produced in the laboratory of our establishment.

4. Experimental techiques and results

The cold-flow experiments have been made to eliminate effects that can be produced by chemical reaction or cooling of hot gases. It was looked for purely aerodynamic causes of side-force generation during gas flow through the motor. In this program converging angle, distance between nozzle entrance and charge simulator, nozzle contour, charge channel width and position of charge channel axis relative to the nozzle axis have been varied.

All experiments show no side-force effects (Fig. 4) besides that configurations where the charge channel is parallely offset from the nozzle axis. To eliminate effects of misadjustment of the wires on the nozzle wall, the tests were performed with the charge axis lying above and below the nozzle axis and thus evaluating only the distance between the Machwave intersection points of such two configurations.

It can be stated that for cold-flow conditions well fabricated nozzles with smooth nozzle surface show no side-forces, as long as the profile of the mass-flow is axisymmetric with respect to the nozzle axis. Any parallel or angular deviation off this conditions results in side-forces. The origin of them comes of the subsonic region. Originally parallel deviations turn over into an angular deviation. Angular deviations create an oscillating flow in the supersonic region. As the "Schlieren"-pictures indicate the oscillation damps out and increases in period length downstream the supersonic nozzle portion. (Fig. 4).

Calculations made from velocity differences deduced from Mach-wave angle measurements close to the nozzle wall result in a side-force diagram, plotted over the nozzle length as shown in the slide. (Fig. 5).

As various nozzle geometries have been used, another noticeable observation was made. The flow behaviour explained before led to the idea that elongation of the nozzle throat to a channel with throat diameter might diminish the

angular deviation of mass-flow. Therefore a nozzle with a channel of a length of 1.8 d_t was investigated. A remarkable reduction of side-forces was observed. Fig. 6 shows the comparsion between a nozzle with a channel at the throat and one without it.

By the cold-flow program the purely aerodynamic side of the problem thus is clarified. The following rocket motor firings had to aim at the phenomena originating from thermodynamic and chemical properties of the combustion gas. So it was looked for a clean aerodynamic shape inside the combustion chamber and of the exhaust nozzle. The design result is shown in Fig. 7 which gives the cross-section of rocket motor.

The propellant charge is of the "international-burning" type and open towards the nozzle entrance in the fashion of a low angle subsonic diffusor with steady cross-section increase up to chamer diameter.

In fact there is a mass-flow increase with increase of cross-section area. Fig. 8 shows the development of gas velocity ($\bar{w} = w/a$) along the motor charge. During the gas flow towards the nozzle no eddys or turbulence should occur therefore. During the test-program three different nozzles have been used. They are shown in Fig. 9 (normal, "channel throat", sonic).

Fig. 10 shows the pressure vs. time record and the two side-force vs. time records of a motor firing. This picture is typical for all firings that have been performed. With respect to the lateral forces three regimes can be recognised, depicted as A, B and C. The regimes A and C are connected to pressure built-up and decay at the beginning and at the end of burning-time. In between both side-force traces oscillate without any predominating frequency. The picture of the side-force traces vary from one firing to the other, but in principle they show the same result.

From this it must be stated, that lateral thrust is always generated during rocket motor firings even if the nozzle is fully flowing and no jet separation can occur and the design of internal gas flow is aerodynamically as clean as possible. The side-forces measured with composite charges show peak-values in the order of half a percent of the axial thrust of the rocket motor. These peak-values always are in the same order of magnitude for charges of the same shape and propellant. Likewise the time-mean values of the side-forces for the entire burning-time are characteristic for certain charge-types.

It was stated that the time-mean-and peak-values for the used double-base charges are only about half as great as for the composite propellant charges. As said before the reason for this can be that the composite-propellant fabricated in the laboratory in small quantities have not been mixed and prepared so well than the double-base slabs coming off an industrial production. But another possible reason may lie in the basic difference in combustion-mechanism with double-base and composite-propellants. It is imaginable that the combustion of a heterogeneous propellant with granular inserts creates stronger irregularities in reaction than a widely homogeneous propellant like the double-base types. At this time no special investigations have been performed to look after this questions.

The tests ran with a nozzle having a channel at the throat with a length of again 1.8 d_t brought a reduction of the lateral thrust components. The remaining peak-values are in the order of 0.1 % of axial motor-thrust for composite as well as for double-base charges. This shows that the damp-

ing concept for side-forces developed in the cold-flow program has works with rocket motors. From this it also can be deduced about the causes of the side-forces in rocket motor firings are non-axisymmetric mass-flow profiles in the subsonic portion of the nozzle. At this time it cannot be explained with certainty which kind of phenomena to occur inside the chamber. But considering that due to internal motor design aerodynamic disturbances are unlikely to arise and that obvious differences in side-forces magnitude exist between different charges, the possible causes concentrate upon influences from the combustion process , i.e. uncomplete combustion with or without afterburning.

Furtheron it is noticed that the peak-values of lateral thrust are equally great with the "channel-throat" nozzle for both types of propellants, whereas with the normal nozzle clear differences exist. Although a sound verification by a large test program including more varintions has not been performed, it is felt that the ratio of length to diameter of the dampingchannel sets a lower limit below which the damping effect of the channel rapidly vanishes.

Several motor firings with double-base charges have been made using a sonic nozzle, i.e. without the supersonic, divergent portion. (Fig. 11). The picture of the side-force traces look very much like those got with a normal supersonic nozzle. From this again it can be deduced that the causes for lateral thrust of that random type is located inside the combustion chamber and the least no essential side-forces are generated in the supersonic portion of the nozzle.

The main object of the firings with this nozzle was to show that the lateral thrust arising during chamber pressure decay at burn-out must be attributed to jet separation in the supersonic nozzle portion. As the side-force records show there are no more large lateral thrust components at burn-out when a sonic nozzle is applied, jet separation is the only cause for high side-forces during pressure decay.

As it is shown in Fig. 10 strong side-forces are generated during the period of pressure decay. These forces are caused by the jet separation off the wall due to too low pressure in the combustion chamber. This is a well-known phenomena. The pressure, at which the separation begins, is defined by the "Summerfield" criterium. As tests have shown, the pressure according to the "Summerfield" criterium can be lowered by the use of a "channel throat", but the appearance or magnitude cannot be diminished by this. In the present phase of investigation we are looking after some technical means that might be able to avoid these side-forces.

The most difficult part of the side-force investigations is that of regime A. Here we are still doing experiments to find the cause of the side-forces. A possible cause can be unequal pressure distribution in the combustion chamber generated by the igniter charge for the propellant slab.

Conclusions

By a rocket motor fired to propel a missile the thrust generated shows lateral thrust components, which can influence the flight trajectory to a remarkable degree and apply loads onto the structure that may generate vibrations or shocks of a considerable strength. High forces notified at burnout of stage may be attributed to the random lateral thrust forces. Cold flow tests and lateral thrust measurements during rocket motor firing clearly demonstrate three different regimes of side-force appearance. Two of them are easily identified as gasdynamic effects due to off-design conditions in the chamber and for the nozzle-flow.

Besides these expected phenomena lateral thrust was observed throughout the entire burning-time with varying direction and magnitude. It was possible to locate the origin of the side-force generating disturbances as occuring in the subsonic portion of the motor and the nozzle. It is fairly obvious that they are due to irregularities of the chemical reaction mechanism during combustion.

Furtheron a method of damping down the peak-values was developed and successfully tested.

The program performed so far comprises only a few points, while the investigation of the influence of a number of parameters is still to be done. Especially as far as damping methods are concerned systematic investigations will lead to still considerable improvements.

Finally it is shown that some basic improvements should be worked out, if the misdistance of unguided missiles shall be reduced. The order of magnitude of leteral thrust observed is sufficient to create considerable flight path alterations.